

ACR April 1938



4 MAR 1948

NATIONAL ADVISORY COMMITTEE FOR AERONAUTICS

WARTIME REPORT

ORIGINALLY ISSUED
April 1938 as
Advance Confidential Report

AERODYNAMIC CHARACTERISTICS OF A 4-ENGINE MONOPLANE

SHOWING EFFECTS OF ENCLOSING THE ENGINES IN

THE WING AND COMPARISONS OF TRACTOR- AND

PUSHER-PROPELLER ARRANGEMENTS

By Abe Silverstein and Herbert A. Wilson, Jr.

Langley Memorial Aeronautical Laboratory
Langley Field, Va.

NACA

WASHINGTON

NACA LIBRARY
LANGLEY MEMORIAL AERONAUTICAL
LABORATORY
Langley Field, Va.

NACA WARTIME REPORTS are reprints of papers originally issued to provide rapid distribution of advance research results to an authorized group requiring them for the war effort. They were previously held under a security status but are now unclassified. Some of these reports were not technically edited. All have been reproduced without change in order to expedite general distribution.

AERODYNAMIC CHARACTERISTICS OF A 4-ENGINE MONOPLANE

SHOWING EFFECTS OF ENCLOSING THE ENGINES IN

THE WING AND COMPARISONS OF TRACTOR- AND

PUSHER-PROPELLER ARRANGEMENTS

By Abe Silverstein and Herbert A. Wilson, Jr.

SUMMARY

Tests have been conducted in the N.A.C.A. full-scale wind tunnel on a 1/4-scale model of a large 4-engine monoplane to determine the over-all aerodynamic efficiency of a conventional wing-nacelle-engine installation as compared with power-plant installations enclosed in the wing with extension shafts to the propellers. The enclosed-engine arrangements were tested with the propellers located in one pusher and in three tractor positions. The results indicate that the addition of the four nacelles, exclusive of radiators, for liquid-cooled engines to the bare wing of the model increases the high-speed drag coefficient by 9 percent, decreases the maximum lift coefficient with flaps down by 7 percent, and markedly reduces the maximum L/D ratio. In contrast, addition of the extension shafts for the enclosed-engine arrangements does not appreciably affect the aerodynamic characteristics of the bare-wing model.

Radiators enclosed in ducts attached to the bottom of the liquid-cooled engine nacelles in combination with oil coolers in the nose of the wing increase the drag of the bare model by 20 percent.

The propulsive efficiencies of the enclosed-engine arrangement are higher than those of the wing-nacelle installation, particularly in the climb condition. The best tractor and the pusher positions are of about equal merit.

INTRODUCTION

An obvious refinement for modern multiengine airplanes is the removal of exposed wing nacelles and radiators and the enclosure of the complete power plant within the wing. The necessity for reduction of engine-nacelle and radiator drag has become increasingly accentuated ow-

ing to the gradual elimination of other sources of parasite resistance. Significant improvement in the performance of present-day airplane types will largely depend, therefore, on the development of more efficient power-plant installations.

In order to determine the effect on the performance of a typical airplane that would follow from enclosing the engines in the wing and removing the exposed radiators, an investigation has been conducted in the N.A.C.A. full-scale wind tunnel of a 1/4-scale model of a large 4-engine monoplane. Representative of conventional design, this model was equipped with four wing nacelles for liquid-cooled engines with external radiators in short ducts under the nacelles and oil radiators in the leading edge of the wing. After the tests of this arrangement, the external nacelles and radiators were removed and the propellers were driven by means of extension shafts from motors located within the wing.

The investigation included measurements of the lift, the drag, and the pitching-moment coefficients of the model and, where appropriate, of the propulsive efficiency of the engine-propeller installations for the following model conditions:

- A. Without nacelles or radiators (fig. 1).
- B. With conventional liquid-cooled engine nacelles and propellers at an average position of 0.39c ahead of the wing leading edge (c is the wing chord at the nacelle location).
 - 1. With external radiators in ducts (fig. 2) and oil coolers in leading edge of the wing.
 - 2. Without radiators and oil coolers.
- C. With motors enclosed in the wing and pusher propellers driven by extension shafts (fig. 3).
- D. With motors enclosed in the wings and tractor propellers driven by extension shafts.

1. Propellers located about 0.39c ahead of the leading edge of the wing (tractor position 1). Extension-shaft housings 4 inches in diameter (fig. 4).
2. Propellers located about 0.26c ahead of the leading edge of the wing (tractor position 2).
 - a. Extension-shaft housings 4 inches in diameter.
 - b. Extension-shaft housings 8 inches in diameter to represent air-cooled engine cowlings on the same airplane scaled to 100 tons gross weight (fig. 5).
3. Propellers located about 0.13c ahead of the leading edge of the wing (tractor position 3).
 - a. Extension-shaft housings 4 inches in diameter (fig. 6).
 - b. Extension-shaft housings 8 inches in diameter.

E. Wing alone without fuselage or nacelles.

For all the arrangements with motors enclosed in the wing, there were no radiators on the model. For convenience of reference, arrangements with enclosed motors and extension shafts to propellers have been designated by the propeller position, e.g., pusher, tractor position 1, etc.

SYMBOLS

- α_T , angle of attack of the fuselage reference axis relative to the wind axis, deg.
- q, dynamic pressure, lb. per sq. ft.
- S, Wing area, sq. ft.
- \bar{c} , mean chord of the wing, area/span, ft.

4

V, air speed, f.p.s.

L, lift, or force normal to the relative wind, lb.

D, drag, or force parallel to the relative wind, lb.

D_c, power-off drag of combination, lb.

R, resultant drag force of a propeller-body combination, lb.

T, thrust of propellers operating in front of a body (tension in propeller shafts), lb.

M, pitching moment, lb.-ft.

ΔD, increase in drag of the body behind the propellers due to the action of the propellers.

T - ΔD, effective thrust of the propeller-body combination.

$$C_L = L/qS$$

$$C_D = D/qS \quad (\text{Subscript } w \text{ refers to power-off drag of the model with } \underline{\text{bare wing}}; c, \text{ to power-off drag of the model with } \underline{\text{engine-propeller arrangement}}; h.s., \text{ to drag at high speed; min, to minimum drag.})$$

$$C_m = M/qS\bar{c}$$

P, total power input to propellers.

$$\eta = \frac{(T - \Delta D) V}{P} = \text{propulsive efficiency.}$$

$$\eta_t = \eta \left(\frac{C_{Dw}}{C_{Dc}} \right) = \text{over-all efficiency.}$$

$$T_{c_o}' = \frac{P \eta_o}{\frac{1}{2} \rho V^3 S} = \text{index thrust coefficient.}$$

$$\eta_o = \eta \text{ at } C_L = 0.25$$

n, propeller revolution speed, r.p.s.

- D, propeller diameter, ft.
- β , propeller blade angle at 0.75 R, deg.
- δ_e , angle of the elevator to the stabilizer (positive when trailing edge of elevator is down), deg.
- δ_f , flap deflection from closed position, deg.
- i_w, i_s , angle of wing and stabilizer setting, respectively, to the reference axis, deg.
- a, slope of lift curve, $dC_L/d\alpha$.

AIRPLANE AND TEST EQUIPMENT

The tests were conducted in the N.A.C.A. full-scale wind tunnel, a description of which is given in reference 1.

The model was a metal-covered, midwing monoplane with a span of 37.25 feet. The wing sections were symmetrical and tapered in thickness from 0.18c at the root to 0.10c at the tip. The wing had a plan form tapered 4:1, with a root chord of 7.28 feet and an area of 172 square feet. Split trailing-edge flaps with an average chord of 0.15c extended over the middle 60 percent of the span with the exception of a short gap at the fuselage. The angle of wing setting to the fuselage reference line was 4.6° . A line diagram of the model, exclusive of the tail, with dimensions of the various nacelle-propeller arrangements tested, is shown in figure 7.

Each propeller was driven by a 25-horsepower squirrel-cage induction motor. The speed of the motors was regulated by varying the impressed frequency and was measured by a Weston electrical tachometer. In order that the motor torques might be computed, the motors were calibrated on a dynamometer to determine the power output from the measured electrical input for various combinations of impressed voltage and frequency.

The motors for the wing-nacelle arrangement were supported in the nacelles ahead of the leading edge of the wing; for the enclosed-engine arrangements, the motors were mounted within the wing between the front and rear spars (fig. 4). The propeller axes for the wing-nacelle

arrangement were parallel to the fuselage reference axis, at an angle of -4.6° with the wing chord line, whereas the thrust axes for the enclosed-engine arrangements lie along the wing chord line. The difference was tolerated to aid in a clean design for the extension-shaft arrangements.

The extension shafts for the enclosed-engine arrangements were supported by tubular housings 4 inches in diameter which were bolted to either the front or the rear spar of the model.

Wood fairings 8 inches in diameter were placed concentrically over the 4-inch housings for some of the tests to simulate air-cooled engine nacelles for the case of a hypothetical 100-ton airplane.

Four 3-blade aluminum-alloy propellers 39 inches in diameter were used throughout the tests; the dimensions of the blades are given in figure 8. Blade settings are given with reference to the 0.75 R station.

TESTS

Power-off measurements of forces and pitching moments were made for all the test arrangements over an angle-of-attack range from zero lift through the stall at an air speed of about 60 miles per hour. Scale effects on the over-all airplane drag and on the drag of the radiators, spinners, nacelles, and extension shafts were obtained in the low angle-of-attack range at air speeds from 30 to 120 miles per hour. Tests of the model with a bare wing (without nacelles, extension shafts, etc.) were made twice during the investigation to isolate the effects of suspected variations in the smoothness of the wing surface. Support tares and interferences were measured over the test range of tunnel speeds and angles of attack.

The nature and the spread of the wing stall for the cases of the wing-nacelle model and of the wing alone were observed by means of wool tufts glued to the upper wing surface.

In addition to the usual balance readings of force and moment, the power-on tests included measurements of electrical input to the motors and of propeller speed.

Propulsive characteristics for each of the engine-propeller arrangements were determined over the useful V/nD range. For these tests the propeller rotational speed was held constant and the tunnel speed was increased to its maximum value, after which the propeller speed was reduced until zero thrust was reached.

In order to determine the slipstream effect on the lift and pitching-moment coefficients of the pusher and tractor position 1 arrangements over the entire angle-of-attack range, tests were made in which the thrust coefficient was varied from the value required for level flight to the considerably larger values required for take-off.

Measurements of intensity of propeller noise were obtained for the three tractor positions by means of an N.A.C.A. portable sound pressure-level meter, which was located approximately 4 feet ahead of and 30 feet below the propellers.

POWER-OFF CHARACTERISTICS

The lift, the drag, and the pitching-moment coefficients and the L/D ratios for all the arrangements tested are shown in figures 9 to 18. These results were obtained at a test air speed of 59 miles per hour, which corresponds to a Reynolds Number of about 2,500,000 based on the average wing chord of 4.62 feet. The scale effects on the coefficients of minimum drag and of the drag at high speed ($C_L = 0.25$) are shown in figures 19 to 23. Coefficients are based on the wing area of 172 square feet and are corrected for wind-tunnel effects. Pitching-moment coefficients are computed about an assumed center-of-gravity position, shown in figure 7. The important characteristics, such as the minimum drag, the high-speed drag, and the maximum lift coefficients, and the maximum L/D ratios, are summarized in table I.

Drag.— Drag results for the two tests of the model with bare wing are shown in figures 19 and 21 and in table I. It will be noted that there is an appreciable discrepancy in the variation of the drag coefficient with air speed between the two results. This difference is attributed to a variation in the smoothness of the wing surface for the two cases, which was probably caused by removal of the wing covering in order to install the enclosed motors following the tests with the wing nacelles. For the com-

parisons and drag increments given in the report, the bare-wing data that were obtained immediately following the tests of the wing-nacelle condition have been used as a reference for the results of the wing-nacelle tests, and the bare-wing data obtained after the enclosed-engine tests have been used as their references. Fortunately the slope of the scale-effect curves, although differing between the two test groups, showed good agreement within each group of test conditions.

The principal drag comparisons are made between data obtained at a tunnel speed of 100 miles per hour, corresponding to a Reynolds Number of 4,300,000. These comparisons show that the wing nacelles increase the high-speed drag coefficient by an increment of 0.0015, or 8.7 percent. The underslung Prestone radiators and leading-edge oil coolers add 0.0035, or 20.4 percent, so that the total increase in drag due to the exposed power-plant installation is 0.0050, or 29.1 percent.

Drag increments for the extension-shaft installations were small, being in most cases within the experimental accuracy. The shortest extension shaft gave the highest drag increment, as shown by the 4-percent increase in the high-speed drag for position 3 (table I); this result may possibly be attributed to the disturbed flow from the end of the extension shaft as it passes over the wing.

The propeller spinners shown in figure 7 do not appreciably affect either the high-speed or the minimum drag coefficients. The results for the 8-inch cowlings, chosen to represent a 56-inch-diameter air-cooled engine nacelle on the leading edge of a 100-ton airplane, show about a 4- to 5-percent increase in the high-speed drag coefficient.

Maximum lift.— The maximum lift coefficients for all the arrangements tested are summarized in table I. The extension shafts for the enclosed-engine arrangements are apparently not detrimental to the maximum lift; in fact, the pusher arrangement shows an unexplainable higher value of maximum lift coefficient than the bare-wing condition. The lower maximum lift coefficients for the conditions with nacelles on the wing leading edge are caused by nacelle interference; the effect is clearly demonstrated by the tuft observations shown in figures 24 and 25. For the wing-alone condition (fig. 24), the stall progresses uniformly inward from the tips with increasing lift coefficient; whereas, for the wing-nacelle condition (fig. 25),

the stall begins almost simultaneously at the tips and behind the nacelles. For the wing-nacelle arrangement, the two stalled regions unite at an angle of attack of about 12° , after which the lift curve (fig. 10) indicates a general stall for the wing. The flat top of the lift curve is generally characteristic of cases in which nacelle interference exists. Tuft observations were not obtained for the extension-shaft arrangements, but it might be expected that the results would be similar to those for the wing alone.

Maximum L/D ratio.— The maximum L/D ratios in table I show the same general trends indicated by the high-speed drag coefficients and clearly demonstrate that the extension shafts only slightly affect the aerodynamic characteristics of the bare-wing model. The maximum L/D value for the bare-wing model is 19.8, compared with 19.6 for the pusher and 19.0 for the tractor position 1.

The maximum L/D ratio for the wing-nacelle arrangement with external radiator is 16.6, or about 15 percent lower than for the bare-wing model. Similar data were not obtained for this model without radiators.

Pitching moments.— The power-off pitching-moment coefficients and the static longitudinal-stability characteristics of the model do not vary widely for all the arrangements tested. The slopes of the pitching-moment curves for the bare-wing and the enclosed-engine arrangements are slightly higher than those for the wing-nacelle model.

PROPULSIVE AND OVER-ALL EFFICIENCIES

Engine-propeller combinations should be compared by means of an over-all efficiency factor including both drag and propulsive efficiency. In this report the over-all efficiency is defined as the ratio of the power that would be required for the bare-wing model at a given speed, to the power input actually required at this speed for the particular propeller-wing combination.

The over-all efficiency of the bare-wing model is therefore 100 percent and, for an engine-propeller combination, is given by

$$\eta_T = \eta \left(\frac{C_{D_H}}{C_{D_0}} \right)$$

The effective thrust of the propeller-body combination, $T - \Delta D$, is obtained from the measured data by means of the relation

$$R = D_c + \Delta D - T$$

For tests without a wing behind the propeller, $T - \Delta D$ is obtained from measurements of D_c and R for the same angle of attack and dynamic pressure. When the propeller is operated in front of or behind a wing, there are changes in the lift as well as in the drag and jet-boundary corrections that should be credited to or charged against the propeller. The change in lift has been allowed for in these results by determining D_c and R at the same lift coefficient instead of at the same angle of attack. Since higher lift coefficients are reached with power on than off, this method fails in the region of maximum lift; however, it is valid over the remainder of the useful flight range.

Propulsive efficiencies are given for two lift coefficients of the model $C_L = 0.25$ and 0.70 , which corresponds approximately to the lift coefficients for high speed and climb. Of particular interest are the curves of figure 26, comparing the efficiencies for the five principal engine-propeller combinations. A blade angle of $18-1/2^\circ$ was used for the comparative tests inasmuch as it represents approximately the setting required to absorb the available power in the climb condition. At the high-speed lift coefficient (fig. 26), the maximum propulsive efficiencies show a dispersion of only about 2 percent between all the combinations tested; the highest value, nearly 80 percent, is given by the pusher and the lowest value, 78 percent, by the conventional wing-nacelle arrangement. In sharp contrast are the values shown in figure 27 for the climb lift coefficient, in which there is a difference of 8 percent between the highest maximum efficiency, 83 percent for the enclosed-engine tractor position 1, and the lowest maximum efficiency, 75 percent for the conventional wing-nacelle arrangement. The pusher, tractor position 2, and tractor position 3 follow tractor position 1 in decreasing order of merit.

The effect of blade angle for the conventional wing-nacelle arrangement is shown in figure 28. With increasing blade angle, the propulsive efficiency increases up to $\beta = 23-1/2^\circ$ for the high-speed lift coefficient and re-

remains about the same for $\beta = 28-1/2^\circ$. The efficiency at the climb condition increases progressively with increasing blade angle up to $\beta = 28-1/2^\circ$. The effects of blade-angle setting for the enclosed-engine arrangement with tractor propellers at positions 2 and 3 are shown in figures 29 and 30. These data indicate in general that, up to a blade angle of about $28-1/2^\circ$, the propulsive efficiencies remain substantially the same.

A continuation of this investigation to cover a wider range of blade angles may be of interest, particularly for high-speed airplanes for which values of $\beta = 40^\circ$ are not uncommon. Values of the maximum propulsive efficiency for all arrangements are given in table I.

Values of over-all efficiency computed by means of the previously defined formula are given in table I for all arrangements at lift coefficients of 0.25 and 0.70. For the lift coefficient corresponding to high speed, the pusher and tractor positions 1 and 2 have over-all efficiencies of 79 and 78 percent, respectively, whereas the model with the conventional wing nacelles has an over-all efficiency of 60 percent with exposed radiators and 72 percent without radiators. For the lift coefficient corresponding to the climb condition, the efficiencies vary from 78 percent for the best enclosed-engine arrangement to 68 percent for the wing-nacelle arrangement with radiators. No allowance has been made for radiator drag in the over-all efficiencies of the enclosed-engine arrangement.

Faired spinners on the extension shafts appear to have a negligible effect on over-all efficiency. The over-all efficiencies for tractor position 3 were definitely inferior, being 3 percent below those for tractor position 1 at the high-speed condition and 6 percent below at climb.

POWER-ON CHARACTERISTICS

The effect of power on the lift and pitching moments of the model for some of the test conditions is shown in figures 31 to 36. In the presentation of the results, the power-on condition for each test is denoted by the index thrust coefficient T_{co}' . This coefficient is defined by

$$T_{co}' = \frac{T - AD}{qS}$$

and is nondimensional and similar to a drag coefficient. In order to determine the T_{c_0}' corresponding to a given operating condition of the propeller, it was found convenient to replace the effective thrust $T - \Delta D$ by its equivalent $P\eta/V$, where P is the total power to all the propellers. Since η varies only slightly with lift coefficient, it was arbitrarily replaced by η_0 , the propulsive efficiency at $C_L = 0.25$, so that

$$T_{c_0}' = \frac{P\eta_0}{qSV}$$

The variations of lift coefficient with T_{c_0}' for the pusher and tractor position 1 are shown in figures 31 and 32. In both cases the tests were made at a tunnel speed of approximately 30 miles per hour in order to reach large values of T_{c_0}' with the available power. The effect of power in both conditions is similar in that the lift-curve slope and the maximum lift coefficient are increased in almost a linear fashion with increasing values of T_{c_0}' (fig. 33). The effect of power is more pronounced for the tractor-propeller condition, inasmuch as the slipstream velocity over the wing is higher than the inflow velocity for the pusher propellers. Computations indicate that part of the increased lift from the pusher propellers is obtained from boundary-layer control by delaying separation at the trailing edge of the wing.

In figures 34, 35, and 36 the pitching-moment coefficients for the model with conventional wing nacelles, the model pusher, and tractor position 1 are shown over a range of values of T_{c_0}' . The pusher is superior to both of the tractor arrangements with respect not only to greater static stability at the high-speed conditions but also to smaller changes in balance with increasing power. Power has a generally similar effect on the pitching-moment coefficients of tractor position 1 and the wing-nacelle arrangement.

PROPELLER NOISE

Inasmuch as the choice of propeller positions will to some extent be governed by the propeller noise, the meas-

urements of the sound-pressure level obtained for the three enclosed-engine tractor propellers are of interest. The results obtained at a propeller speed of 3,000 r.p.m. are as follows:

Tractor position	Sound pressure, decibels
1	78.5
2	78.3
3	85.5

The discrepancy between positions 1 and 2 is probably within the limits of experimental accuracy. In the tunnel tests, the noise level of position 3 corresponded to a roar as compared to a swish for positions 1 and 2. Unfortunately, data were not obtained for the other test arrangements.

PERFORMANCE COMPARISONS

In order that the merits of the enclosed-engine arrangement may be illustrated, sample performance calculations are presented. The performance of the enclosed-engine arrangement is given only for the case of the pusher arrangement; however, owing to the similarity in the aerodynamic characteristics shown in table I, the computations apply almost equally well to the tractor positions 1 and 2.

High speed.— From the measured drag and propulsive efficiencies, the high speeds were computed for four different model conditions (fig. 37). Computations are based on a wing loading of 25.7 pounds per square foot and a power loading of 17.7 pounds per horsepower. The assumed propeller-blade angle of $18-1/2^\circ$ is lower than the optimum for the high-speed condition, and all the calculated speeds would have been somewhat higher if a larger blade angle had been used. The maximum speeds are as follows:

Condition	High speed m.p.h.
Wing nacelles, tractor:	
1. With exposed radiators - - - - -	194
2. Without radiators - - - - -	207

Condition

**High speed
m.p.h.**

Enclosed engine, pusher:

- | | |
|---------------------------------------|-----|
| 3. With wing-duct radiators - - - - - | 212 |
| 4. Without radiators - - - - - | 218 |

Conditions 2 and 4 offer the most fundamental comparison; it may be noted that the enclosed-engine model has a speed higher by 11 miles per hour. To obtain this same increase in speed by increasing the power would require an engine with 17 percent greater power, even if the secondary effects of the larger power plant on the remainder of the structure are neglected. Of interest is the comparison between cases 1 and 3, from which it may be noted that the high speed is increased 18 miles per hour by using the enclosed-engine arrangement in combination with wing-duct radiators. To obtain a corresponding increase in speed by increasing power would require a 31 percent larger engine. In the comparison of cases 1 and 3, a drag increment of 8 percent was allowed for wing-duct radiators. This estimate is based on preliminary results given in reference 2 and will be subject to revision when more comprehensive data on wing-duct radiators are available.

The gain in high speed resulting from enclosing the power-plant installation is obviously a direct function of the power loading. The foregoing calculations, being based on a relatively high value of power loading in pounds per horsepower, are believed conservative, and still larger gains are available for airplanes designed for high speed rather than long range.

Landing speed.-- If it is assumed, for comparison, that the landing is made at maximum lift with power off, the following table gives the landing speeds for the wing-nacelle and pusher models with flaps both up and down. The airplane is again assumed to have a wing loading of 25.7 pounds per square foot.

Condition	$C_{L_{max}}$	Landing speed m.p.h.
Wing-nacelle model:		
Flaps up - - - - -	1.19	92
Flaps down 60° - - - - -	1.69	77
Enclosed-engine pusher:		
Flaps up - - - - -	1.34	86
Flaps down 60° - - - - -	1.82	74

For the normal landing condition, flaps down, the pusher model has a landing speed lower by 3 miles per hour, or 4 percent, than the model with conventional wing nacelles. For the flap-up condition, the landing speed is decreased about 6 miles per hour. The gains as computed for the pusher model are about the same for all the enclosed-engine arrangements.

Range.-- If the aerodynamic characteristics and the propulsive efficiency of an airplane are known and the assumptions made that the specific fuel consumption, the propulsive efficiency, and the L/D ratio are maintained constant throughout the flight, the range of an airplane may be rather accurately predicted by the simple Breguet formula given as follows:

$$\text{Range in miles} = 863 \frac{L}{D} \frac{\eta}{w_f} \log_{10} \frac{W_1}{W_2}$$

in which

w_f is the specific fuel consumption in pounds per horsepower-hour.

W_1 and W_2 , the initial and final gross weights.

For purposes of comparing the enclosed-engine arrangement and the model with conventional wing nacelles, the values of w_f and of W_1 and W_2 may be taken the same for both arrangements and the maximum range expressed as follows:

$$\text{Maximum range} = k(L/D)_{\max} \eta$$

in which the constant k is the same for both models. The variables are then the maximum value of the L/D and the propulsive efficiency η , which may be taken from the measured data. These values are given in the following table:

Condition	$(L/D)_{\max}$	η , percent
Wing nacelles with external radiators - - - - -	16.6	76
Enclosed-engine pusher with wing-duct radiators - - - -	18.2	80

Substituting the values given in the table into the equation for maximum range,

$$\text{Maximum range}_{\text{tractor}} = 12.6 \text{ k}$$

$$\text{Maximum range}_{\text{pusher}} = 14.6 \text{ k}$$

It is therefore to be observed that the range is increased about 16 percent by converting the model with conventional wing nacelles and external radiators into one with an enclosed engine and wing-duct radiators.

CONCLUDING REMARKS

The measured aerodynamic characteristics of the models with enclosed engines excel those for the model with conventional wing nacelles in all respects. The conventional wing nacelles increase the drag coefficient at the high-speed condition by 8.7 percent, whereas the extension shafts for the better enclosed-engine arrangements add no appreciable drag. From these data and the assumptions of wing and power loadings corresponding to those for a long-range airplane, it has been computed that the high speed of the assumed airplane would be increased about 11 miles per hour by the conversion of the conventional wing-nacelle arrangement into one with the engines enclosed within the wing.

The maximum L/D for the pusher arrangement with wing-duct radiators is 18.2, as compared with a value of 16.6 for the wing-nacelle arrangement with exposed radiators. The propulsive efficiency of one of the better enclosed-engine arrangements, such as the pusher, in the attitude for maximum L/D is 80 percent, as compared with an efficiency of 76 percent for the wing-nacelle model. From a combination of these two factors, the maximum range of the pusher airplane with wing-duct radiators has been estimated to be 16 percent higher than that of the airplane with wing nacelles and exposed radiators.

The foregoing improvements in performance are based on assumptions of wing and power loadings corresponding to those for a long-range airplane and are believed conservative for airplanes designed primarily for high speed.

The results indicate that the enclosed-engine arrangements with tractor propellers 0.26c and 0.39c ahead of the wing and with pusher propellers are of about equal merit; the 0.13c tractor-propeller position, however, shows a definitely lower over-all efficiency.

Langley Memorial Aeronautical Laboratory,
National Advisory Committee for Aeronautics,
Langley Field, Va., February 17, 1938.

REFERENCES

1. DeFrance, Smith J.: The N.A.C.A. Full-Scale Wind Tunnel. NACA Rep. No. 459, 1933.
2. Silverstein, Abe, and Nickle, F. R.: Preliminary Full-Scale Wind-Tunnel Investigation of Wing Ducts for Radiators. NACA ACR, March 1938.

**TABLE I. COMPARISON OF PRINCIPAL AERODYNAMIC CHARACTERISTICS OF MODEL¹
 WITH DIFFERENT MOTOR-PROPELLER ARRANGEMENTS**

Airplane	¹ C _{Dmin}	¹ C _D at C _L = 0.25	C _{Lmax}		(L/D) _{max}	Maximum propulsive efficiency ²		Maximum over-all efficiency ³	
			δ _f = 0°	δ _f = 60°		C _L = 0.25	C _L = 0.70	C _L = 0.25	C _L = 0.70
Wing alone	0.0088	0.0098	1.26	1.77	24.5	-	-	-	-
Bare wing	³ 0.0164 ⁴ 0.0155	³ 0.0173 ⁴ 0.0168	1.29	-	19.8	1.00	1.00	1.00	1.00
Conventional nacelle tractor with radiators	.0208	.0223	1.16	⁵ 1.69	16.6	.78	.75	.60	.68
Conventional nacelle tractor without radi- ators	.0179	.0188	-	-	-	-	-	⁶ .72	-
Pusher; spinners on	.0155	.0168	1.34	1.82	19.6	.80	.80	.79	.77
Pusher; spinners removed	.0155	.0168	1.34	1.79	19.4	.79	.80	.79	.77
Tractor position 1; di- ameter of extension-shaft housing, 4 in.	.0158	.0172	1.28	1.77	19.0	.79	.83	.78	.78
Tractor position 2; di- ameter of extension-shaft housing, 4 in.	.0157	.0170	1.27	1.75	19.0	.79	.79	.78	.74
Tractor position 3; di- ameter of extension-shaft housing, 4 in.	.0162	.0175	1.30	1.74	18.8	.79	.77	.75	.72
Tractor position 2; diam- eter of cowling, 8 in.	.0161	.0177	1.30	-	19.3	.79	.80	.76	.75
Tractor position 3; diam- eter of cowling, 8 in.	.0163	.0175	1.30	1.75	18.7	.78	.78	.76	.72
Tractor position 3; diam- eter of cowling, 8 in.; spinners removed	.0163	.0177	-	-	-	.78	.77	.76	.72

¹ Drag coefficients given are for 100 m.p.h. tunnel speed.

² Blade angle, 18-1/2°.

³ Reference value for conventional nacelle tractor.

⁴ Reference value for enclosed-engine arrangements.

⁵ Landing gear extended; all others, landing gear retracted.

⁶ Based on propulsive efficiency from tests with radiators.

FIGURE LEGENDS

- Figure 1.- Installation of the 4-engine model in the full-scale wind tunnel: Bare-wing case.
- Figure 2.- Installation of the 4-engine model in the full-scale wind tunnel; Conventional nacelles and external radiators for liquid-cooled engines.
- Figure 2(a).- Bottom view - Installation of the 4-engine model in the full-scale wind tunnel: Conventional nacelles and external radiators for liquid-cooled engines.
- Figure 3.- Installation of the 4-engine model in full-scale wind tunnel. Four-inch diameter extension shaft housings and pusher-propeller arrangement.
- Figure 4.- Installation of the 4-engine model in the full-scale wind tunnel: Four-inch-diameter extension-shaft housings and tractor propellers 0.39c ahead of wing.
- Figure 5.- Installation of the 4-engine model in full-scale wind tunnel: Eight-inch-diameter cowls and tractor propellers at 0.26c ahead of wing.
- Figure 6.- Installation of the 4-engine model in the full-scale wind tunnel: Four-inch diameter extension shaft housings and tractor propellers at 0.13c ahead of wing.
- Figure 7.- Diagram of model.
- Figure 8.- Blade dimensions for 3-blade model propellers.
- Figure 9.- Aerodynamic characteristics of model. Bare wing, without nacelles or radiators; $\delta_e, 0^\circ$; $\delta_f, 0^\circ$; approximate test air speed, 59 m.p.h.
- Figure 10.- Aerodynamic characteristics of model. Wing nacelles and radiators for liquid-cooled engines; $\delta_e, 0^\circ$; approximate test air speed, 59 m.p.h.
- Figure 11.- Aerodynamic characteristics of model. Pusher model; housing diameter, 4 inches; spinners on; approximate test air speed, 59 m.p.h.

Figure 12.- Aerodynamic characteristics of model. Pusher model; housing diameter, 4 inches; spinners removed; δ_o , 0° ; approximate test air speed, 59 m.p.h.

Figure 13.- Aerodynamic characteristics of model. Tractor position 1; housing diameter, 4 inches; spinners on; δ_o , 0° ; approximate test air speed, 59 m.p.h.

Figure 14.- Aerodynamic characteristics of model. Tractor position 2; housing diameter, 4 inches; spinners on; δ_e , 0° ; approximate test air speed, 59 m.p.h.

Figure 15.- Aerodynamic characteristics of model. Tractor position 2; cowling diameter, 8 inches; spinners on; δ_o , 0° ; δ_f , 0° ; approximate test air speed, 59 m.p.h.

Figure 16.- Aerodynamic characteristics of model. Tractor position 3; housing diameter, 4 inches; spinners on; δ_f , 0° ; approximate test air speed, 59 m.p.h.

Figure 17.- Aerodynamic characteristics of model. Tractor position 3; cowling diameter, 8 inches; spinners on; δ_o , 0° ; approximate test air speed, 59 m.p.h.

Figure 18.- Aerodynamic characteristics of wing alone without fuselage or nacelles. δ_f , 0° ; approximate test air speed, 59 m.p.h. d/τ , 0.135; l/τ , 0.083.

Figure 19.- Scale effect on the drag coefficient for the models with wing nacelles and radiators and with the bare wing. δ_o , 0° ; δ_f , 0° .

Figure 20.- Scale effect on the increments of drag from nacelle and radiators for the model with wing nacelles and radiators.

Figure 21.- Scale effect on the drag coefficient for the pusher model. δ_e , 0° ; δ_f , 0° .

Figure 22.- Scale effect on the drag coefficient for tractor positions 1, 2, and 3. Diameter of extension-shaft housing, 4 inches; spinners on; δ_e , 0° ; δ_f , 0° .

Figure 23.- Scale effect on the drag coefficient for tractor positions 2 and 3. Cowling diameter, 8 inches; δ_o , 0° ; δ_f , 0° .

Figure 24.- Tuft surveys for the wing alone without fuselage or nacelles. $\delta_e, 0^\circ$; approximate test air speed, 50 m.p.h.

Figure 25.- Tuft surveys for the conventional wing-nacelle model. $\delta_e, 0^\circ$; $\delta_f, 0^\circ$; approximate test air speed, 50 m.p.h.

Figure 26.- Comparison of the propulsive efficiencies of five test arrangements at a lift coefficient corresponding to high speed, $C_L = 0.25$. $\beta, 18\frac{1}{2}^\circ$.

Figure 27.- Comparison of the propulsive efficiencies of five test arrangements at a lift coefficient corresponding to best climb, $C_L = 0.70$. $\beta, 18\frac{1}{2}^\circ$.

Figure 28.- Propulsive efficiencies of wing-nacelle arrangement for four different blade angles.

Figure 29.- Variation of propulsive efficiency with blade angle for propellers in tractor position 2.

Figure 30.- Variation of propulsive efficiency with blade angle for propellers in tractor position 3.

Figure 31.- Effect of power on lift coefficient for the pusher model. $\delta_e, 0^\circ$; $\delta_f, 0^\circ$; approximate test air speed, 30 m.p.h.

Figure 32.- Effect of power on lift coefficient for tractor position 1. $\delta_e, 0^\circ$; $\delta_f, 0^\circ$; approximate test air speed, 30 m.p.h.

Figure 33.- Effect of power on the maximum lift coefficient and on the lift-curve slope for the pusher model and for tractor position 1. $\delta_e, 0^\circ$; $\delta_f, 0^\circ$; approximate test air speed, 30 m.p.h.

Figure 34.- Effect of power on the pitching-moment coefficient for the model with wing nacelles and external radiators. $\delta_e, 0^\circ$; $\delta_f, 0^\circ$.

Figure 35.- Effect of power on the pitching-moment coefficient for the pusher model. $\delta_e, 0^\circ$; $\delta_f, 0^\circ$.

Figure 36.- Effect of power on the pitching-moment coefficient for tractor position 1. $\delta_e, 0^\circ$; $\delta_f, 0^\circ$.

Figure 37.- Comparison of high-speed computations for the wing-nacelle and the pusher models showing the effect of enclosing engines and radiators within the wings. Wing loading, 25.7 pounds per square foot; power loading, 17.7 pounds per horsepower, β , $18\frac{1}{2}^\circ$; standard sea-level density; δ_o , 0° ; δ_f , 0° .

N.A.C.A.

FIG. 1

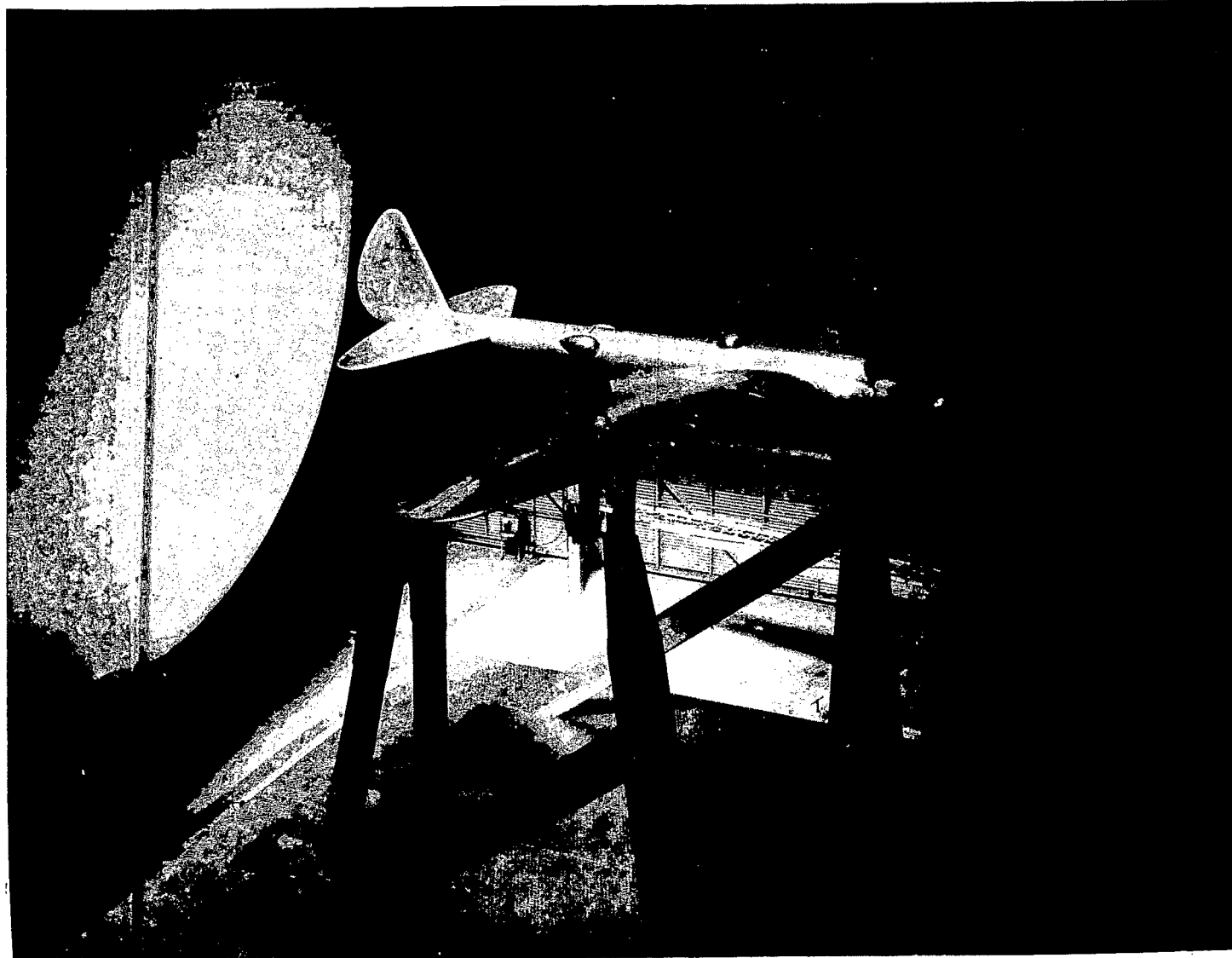


Figure 1.- Installation of the 4-engine model in the full-scale wind tunnel: Bare-wing case.

N.A.C.A.

Figs. 2, 2(a)

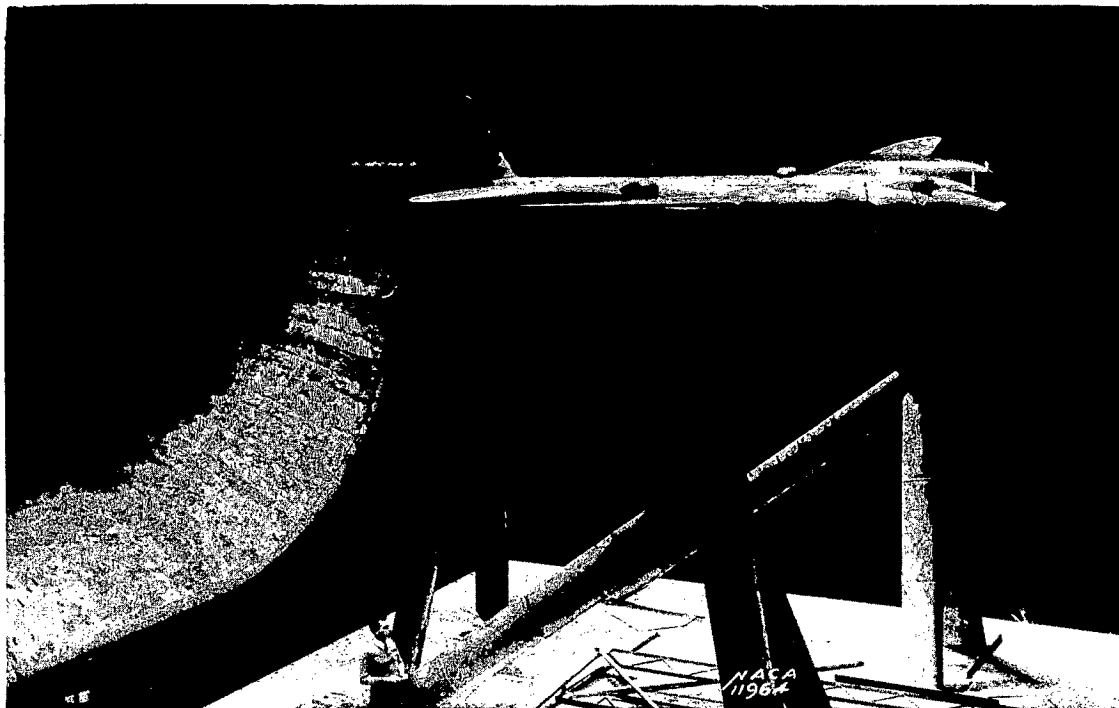


Figure 2.- Installation of the 4-engine model in the full-scale wind tunnel: Conventional nacelles and external radiators for liquid-cooled engines.

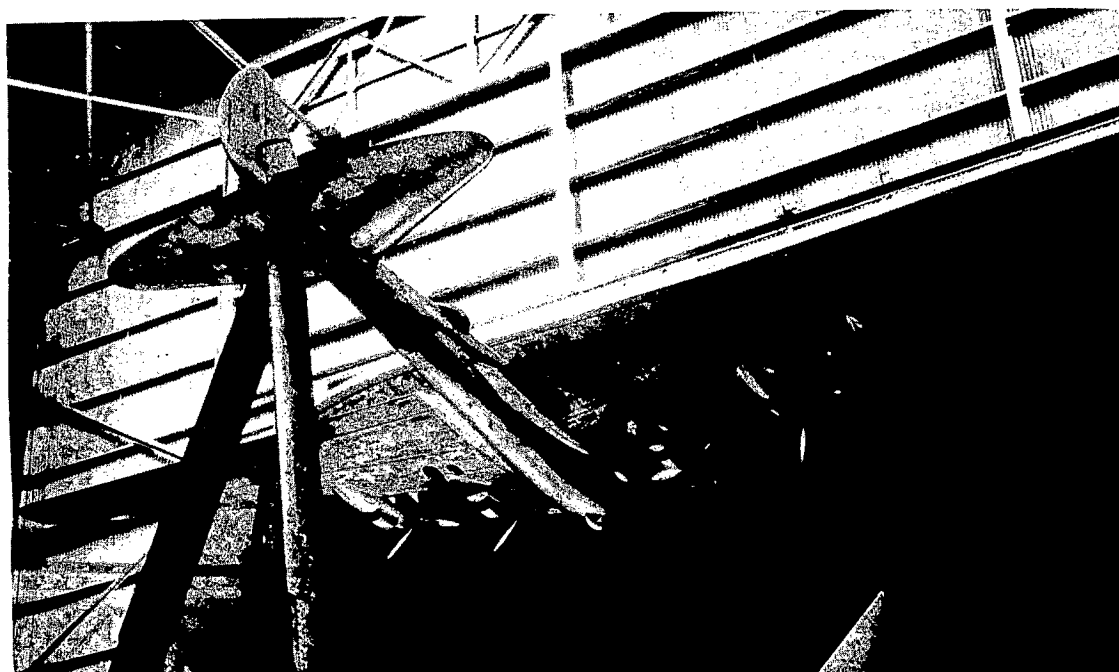


Figure 2(a) Bottom view.- Installation of the 4-engine model in the full-scale wind tunnel: Conventional nacelles and external radiators for liquid-cooled engines.

N.A.C.A.

Figs. 3,4



Figure 3.- Installation of the 4-engine model in full-scale wind tunnel.
Four-inch diameter extension shaft housings and pusher-propeller
arrangement.

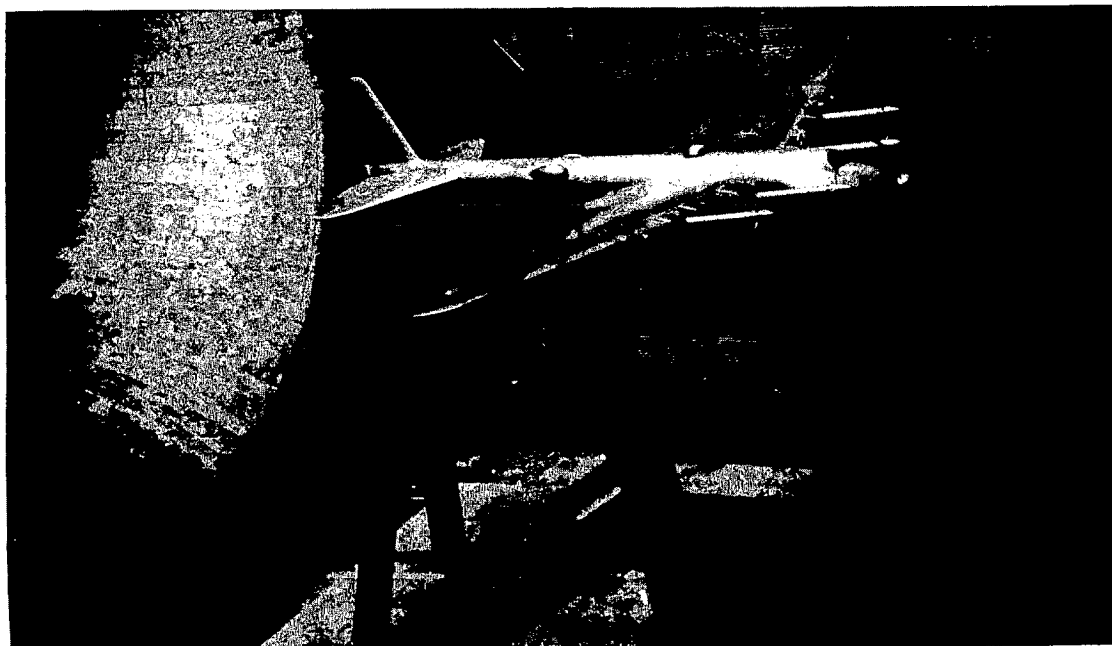


Figure 4.- Installation of the 4-engine model in the full-scale wind tunnel:
Four-inch-diameter extension-shaft housings and tractor propellers
0.39c ahead of wing.

H.A.C.A.

Figs. 5, 6

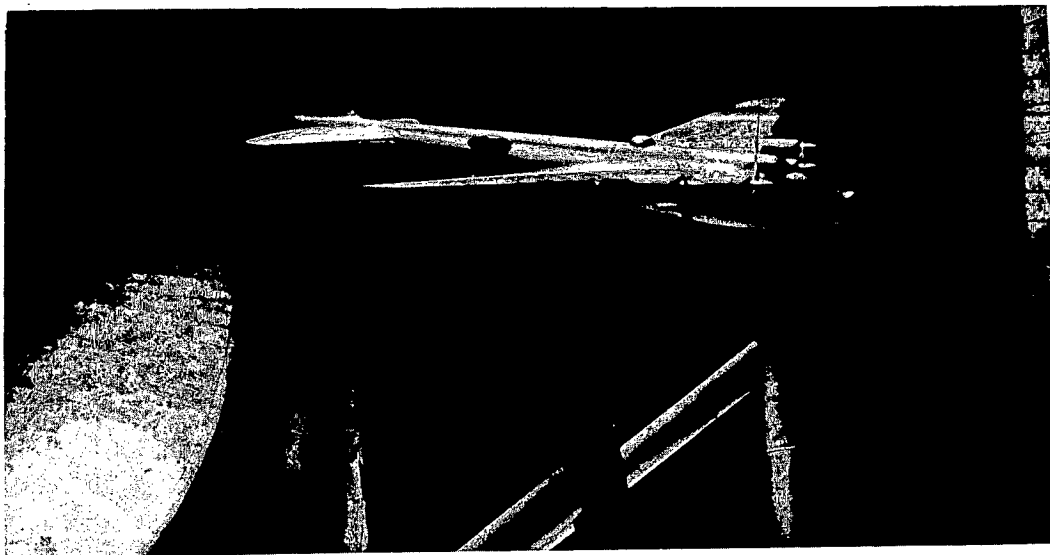


Figure 5.- Installation of the 4-engine model in full-scale wind tunnel:
Eight-inch-diameter cowls and tractor propellers at 0.26c ahead
of wing.

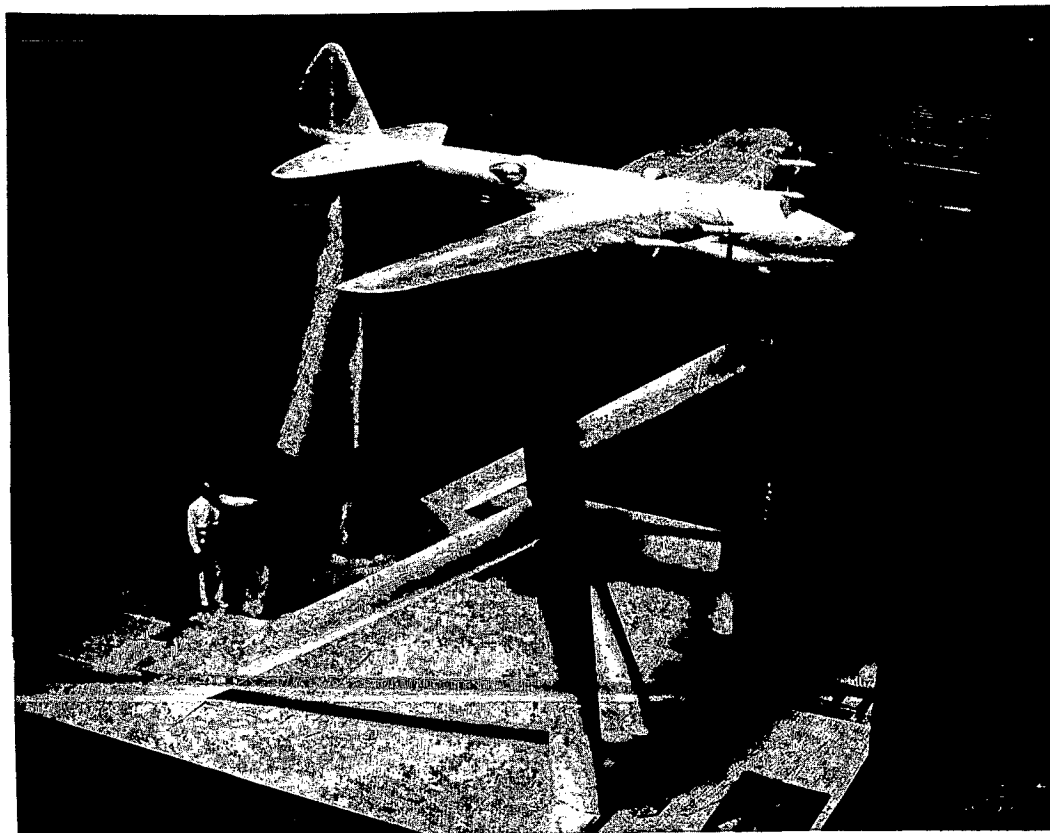


Figure 6.- Installation of the 4-engine model in the full-scale wind tunnel:
Four-inch diameter extension shaft housings and tractor propellers
at 0.13c ahead of wing.

N.A.C.A.

Fig. 7

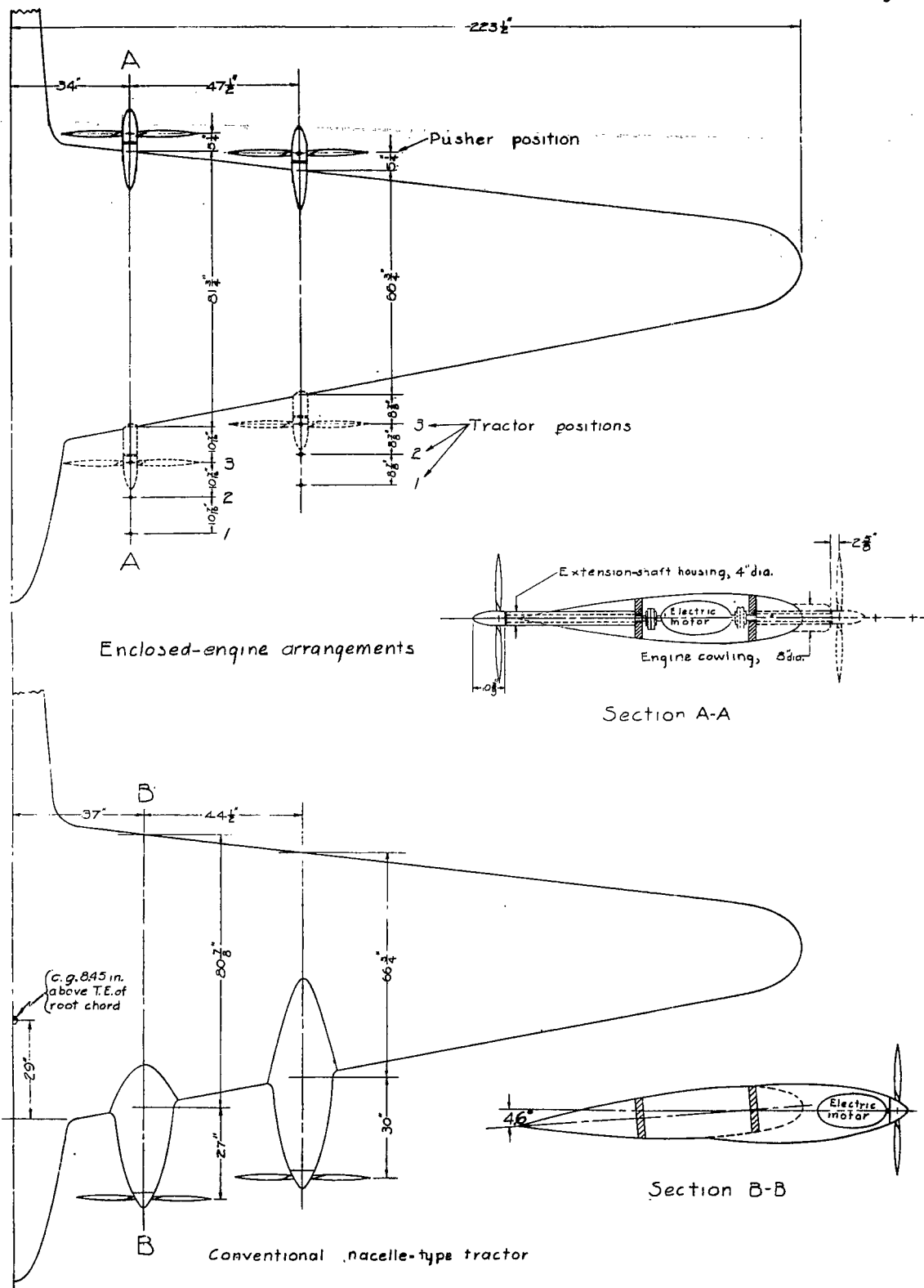


FIG. 7.-DIAGRAM OF MODEL.

N.A.C.A

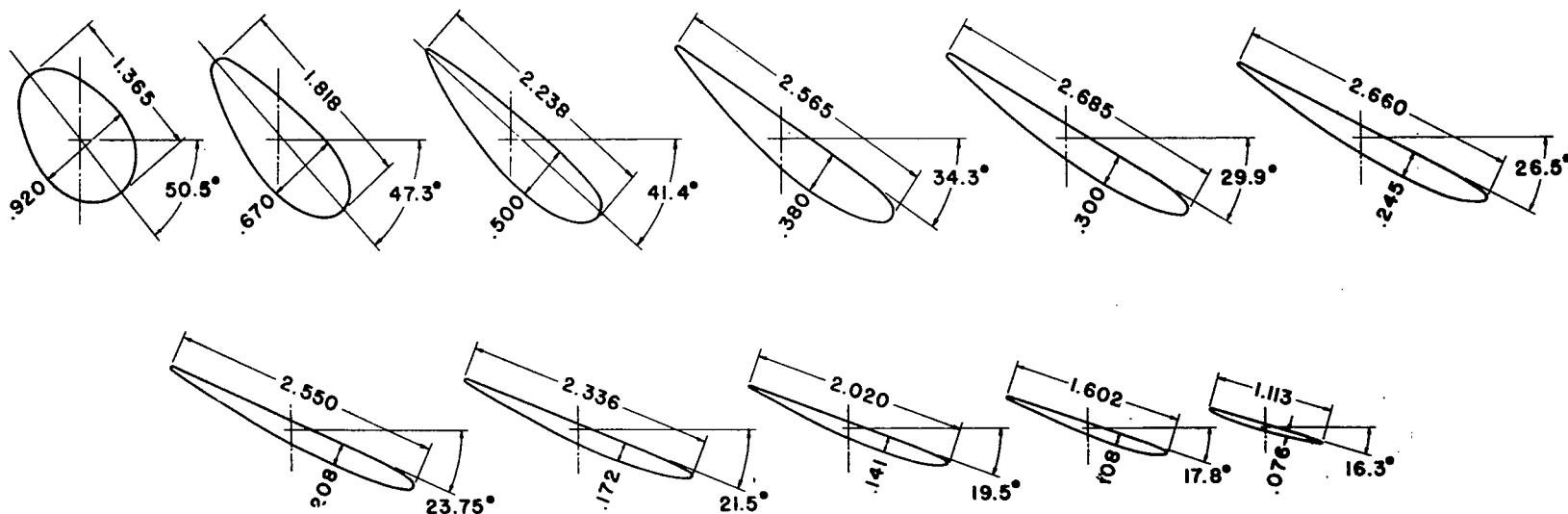
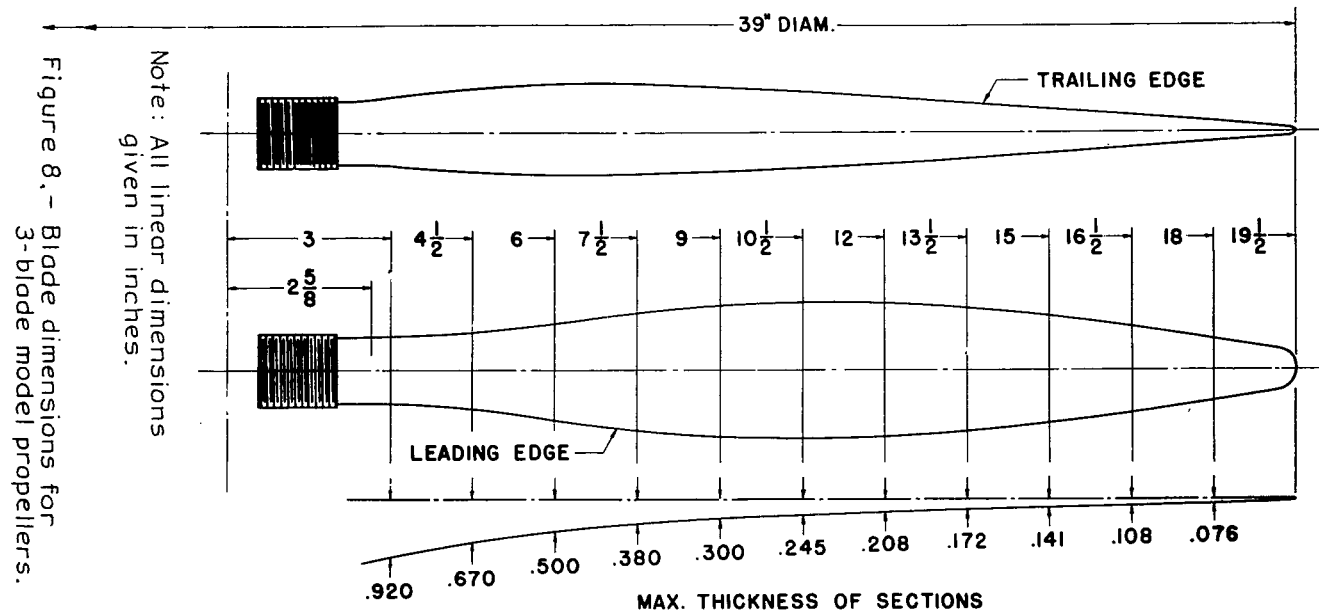


FIG. 8

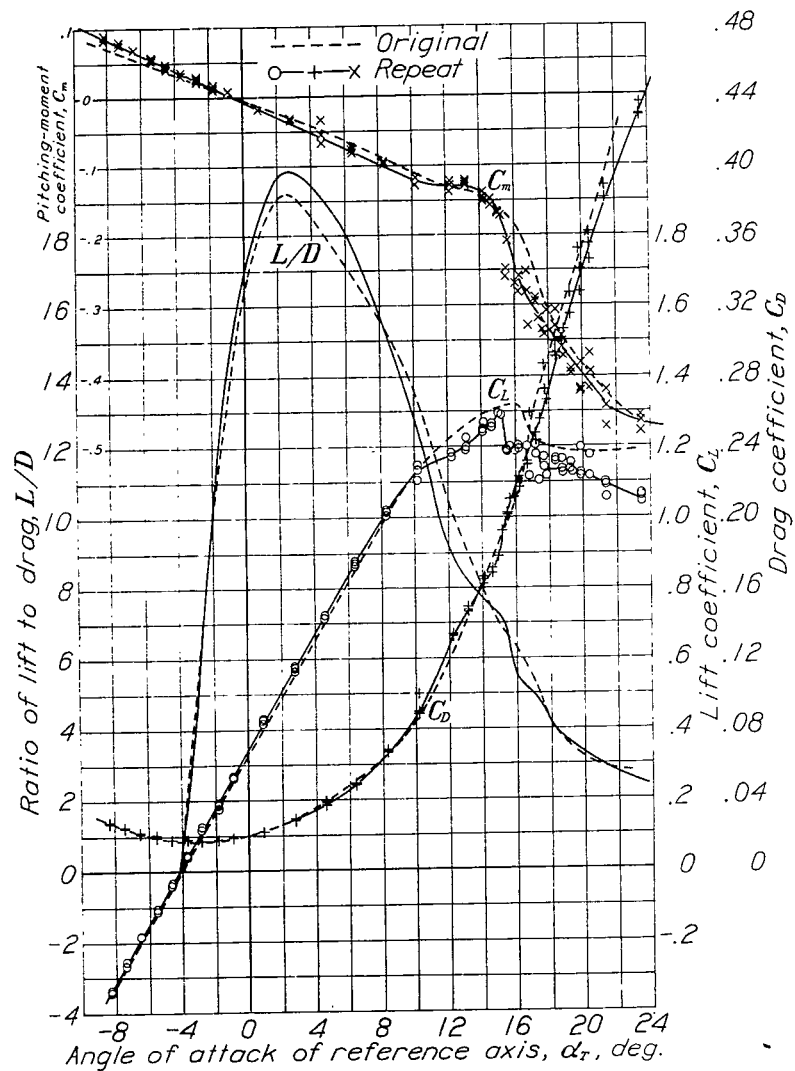


Figure 9

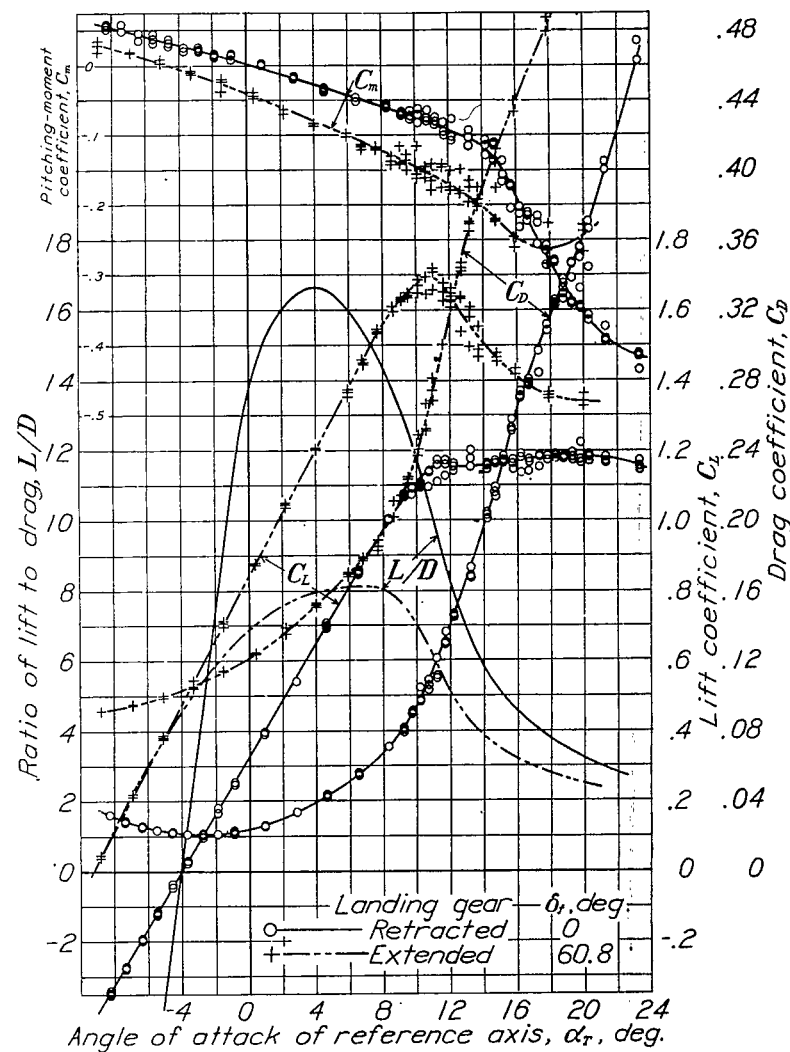


Figure 10

N.A.C.A.

Figs. 9, 10

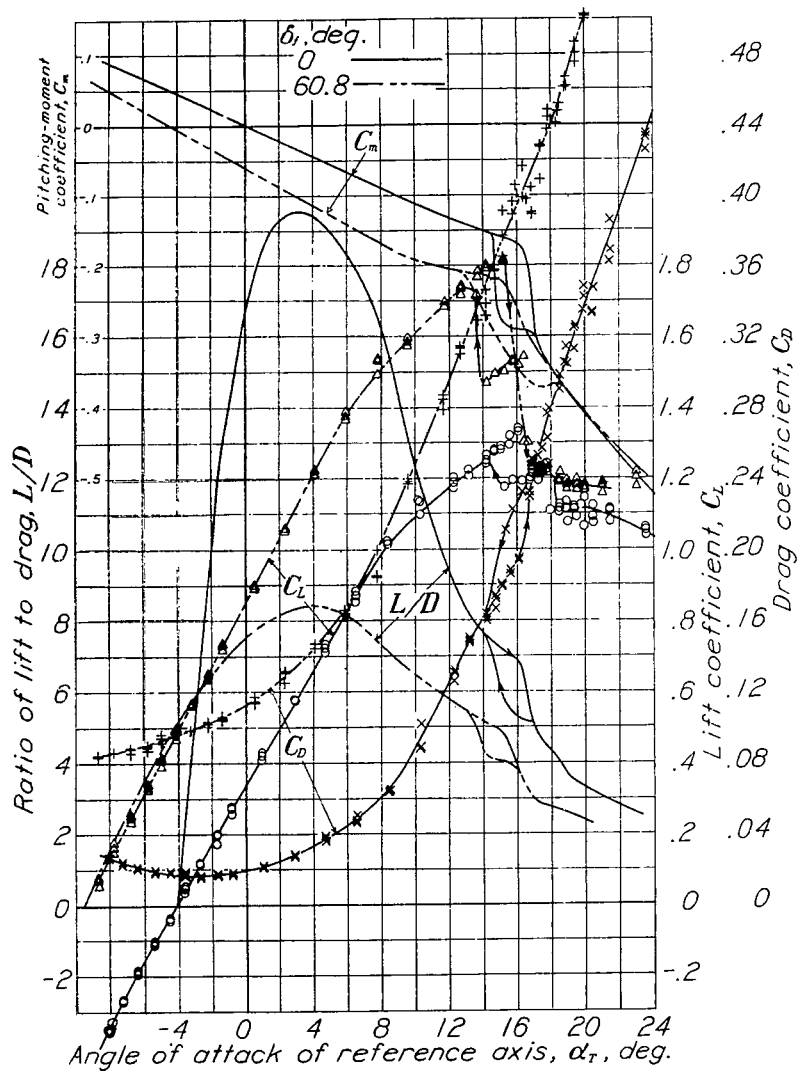


Figure 11

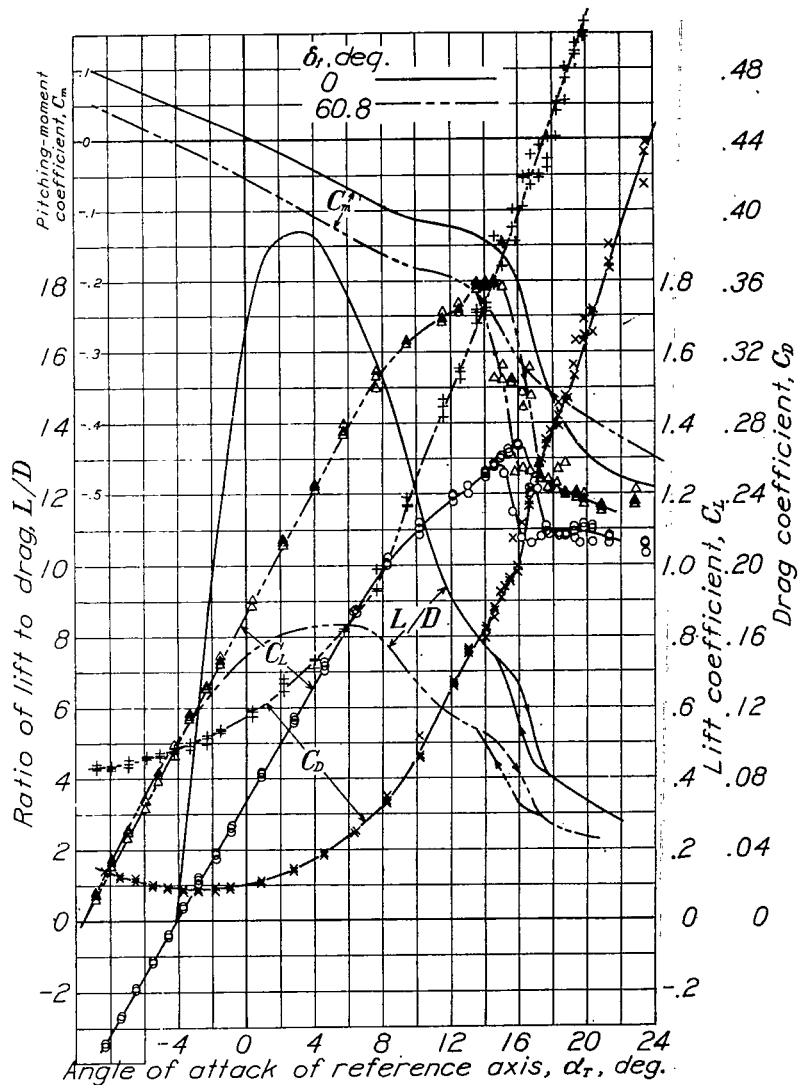


Figure 12

N.A.C.A.

Figs. 11, 12

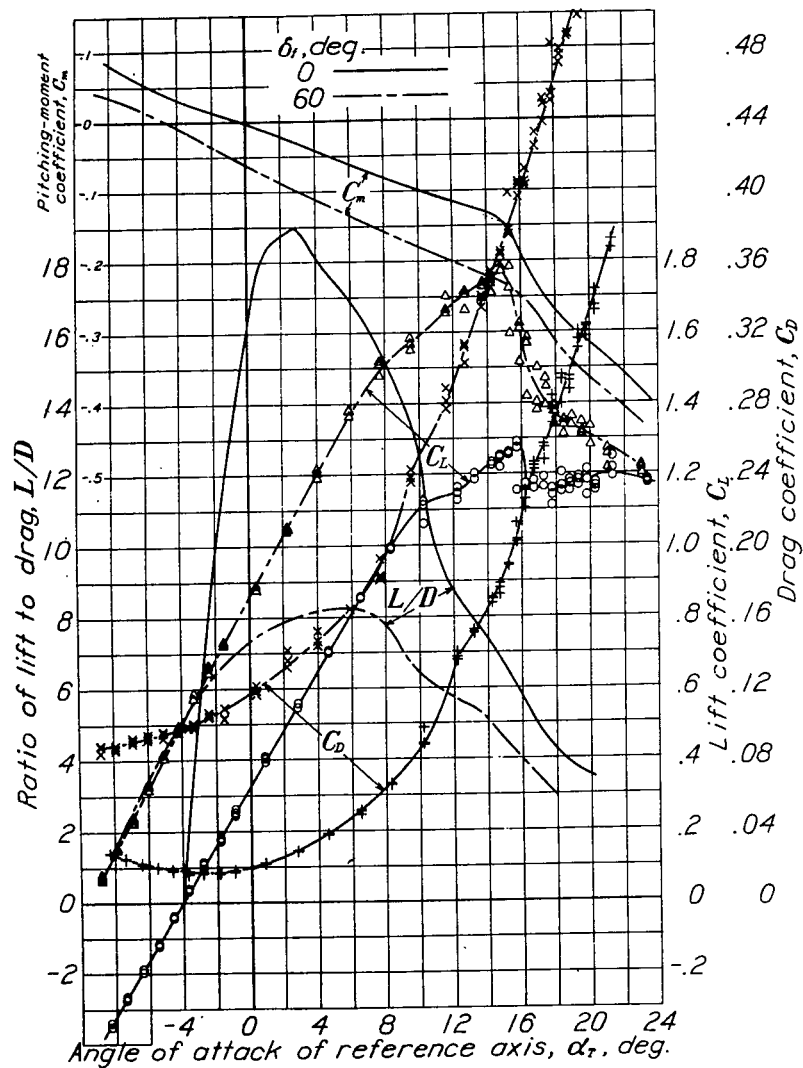


Figure 13

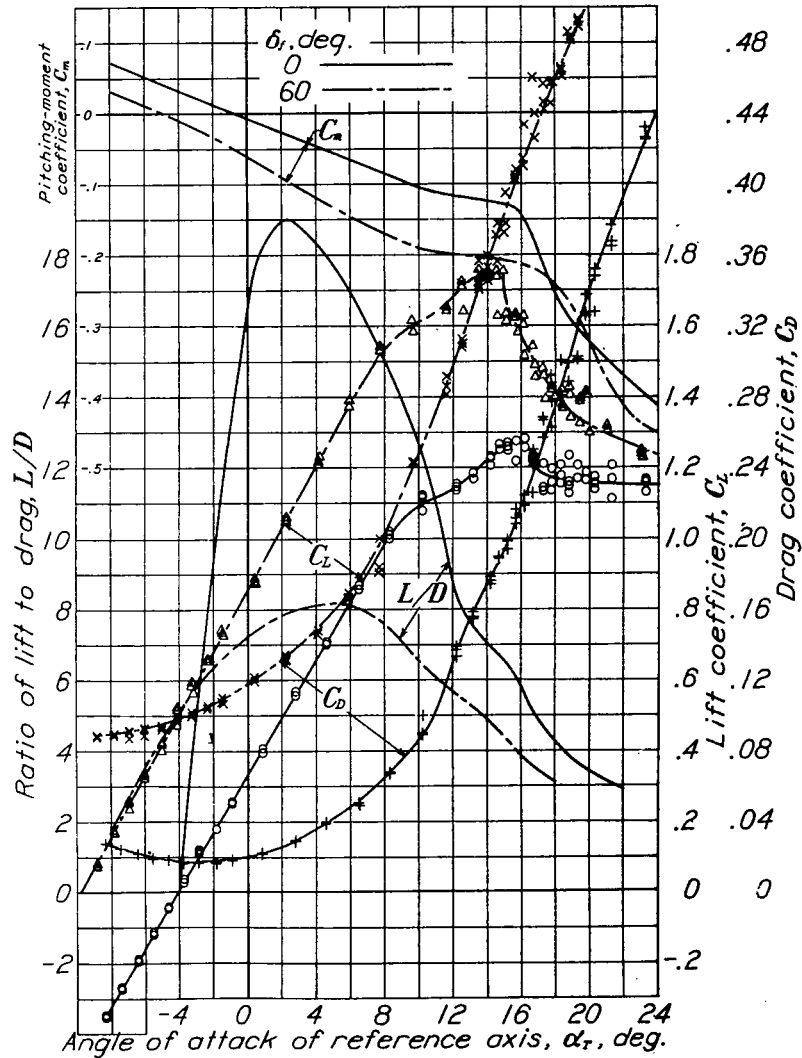


Figure 14

N.A.C.A.

Figs. 13, 14

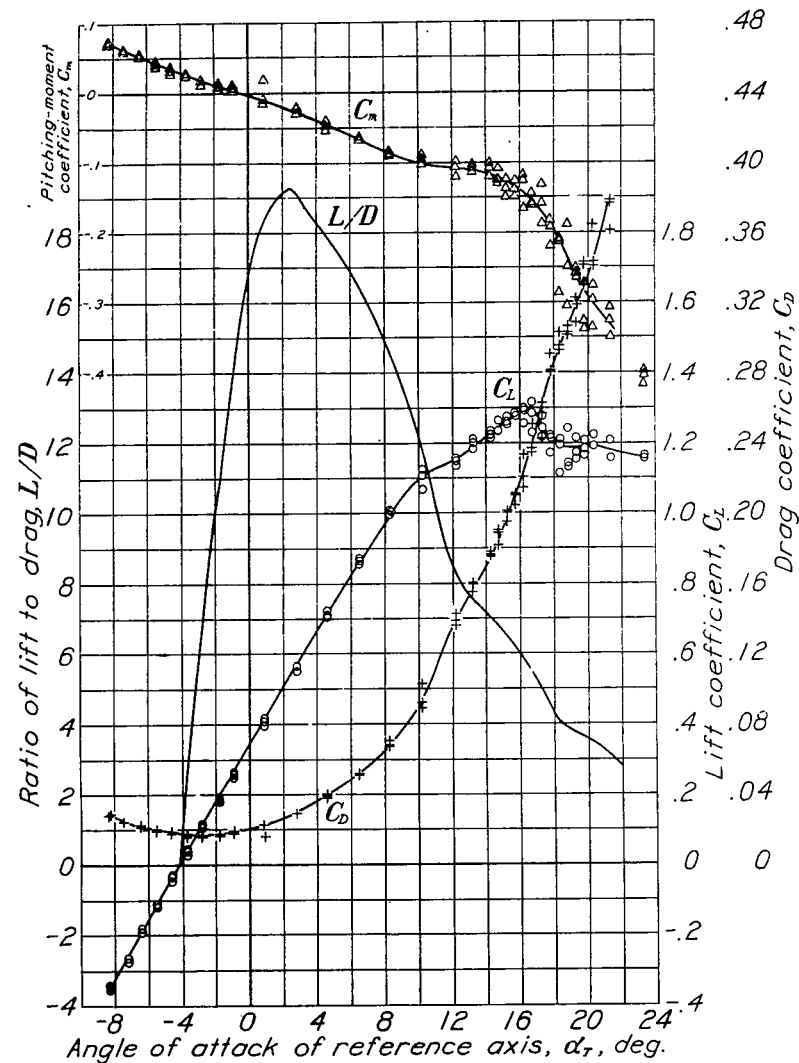


Figure 15

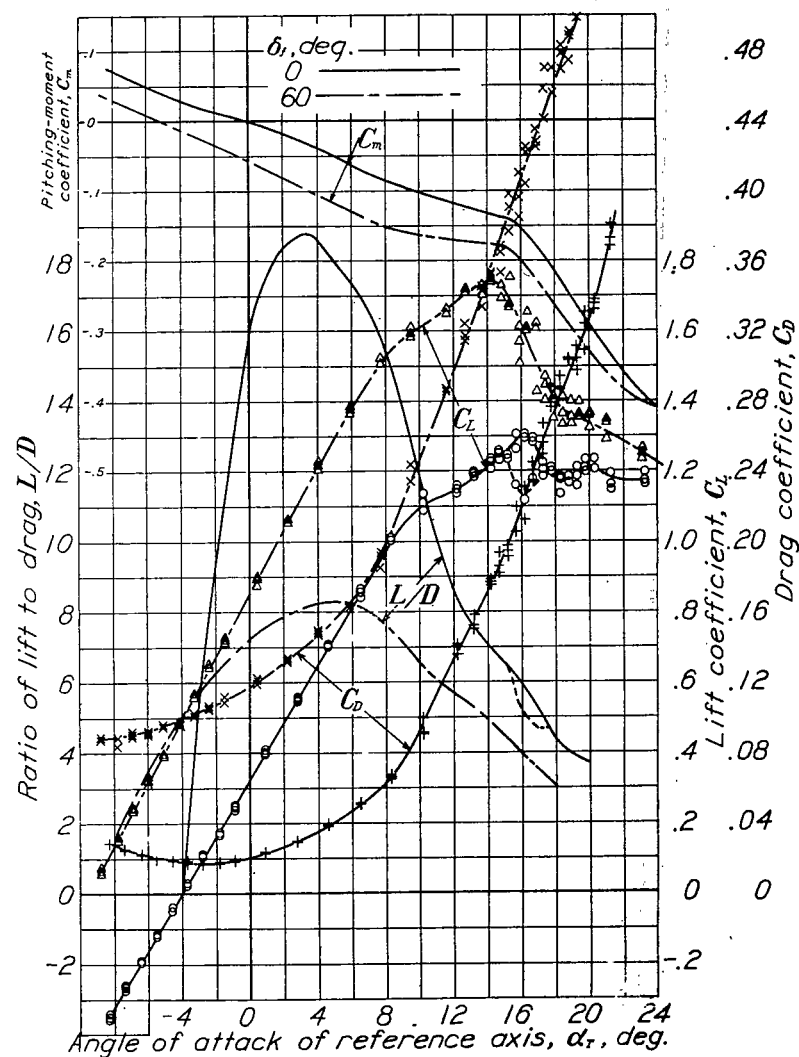


Figure 16

N.A.C.A.

Figs. 15, 16

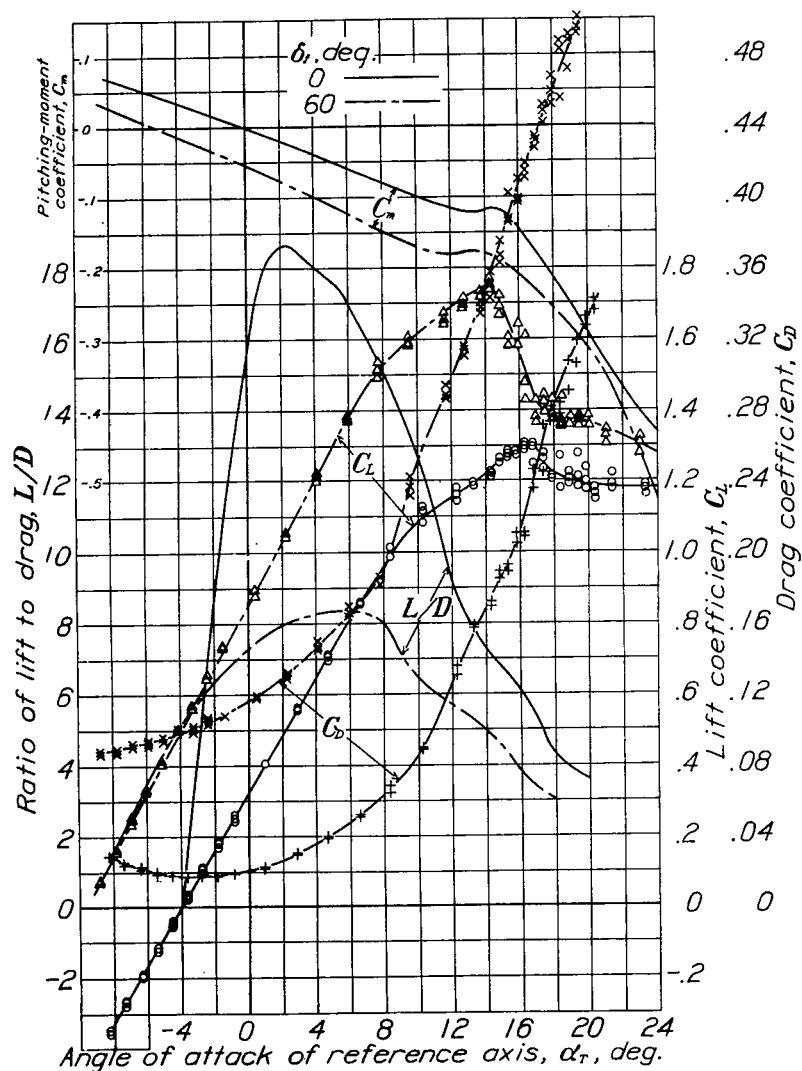


Figure 17

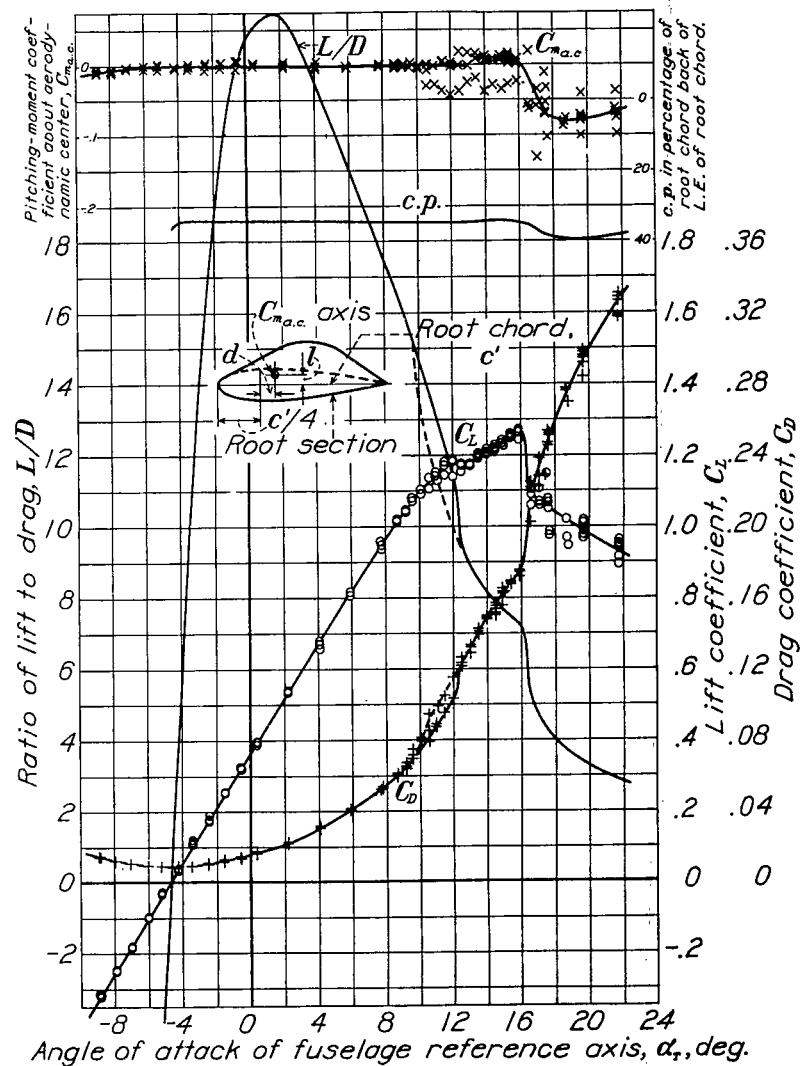


Figure 18

N.A.C.A.

Figs. 17, 18

N.A.C.A.

Figs.19.20

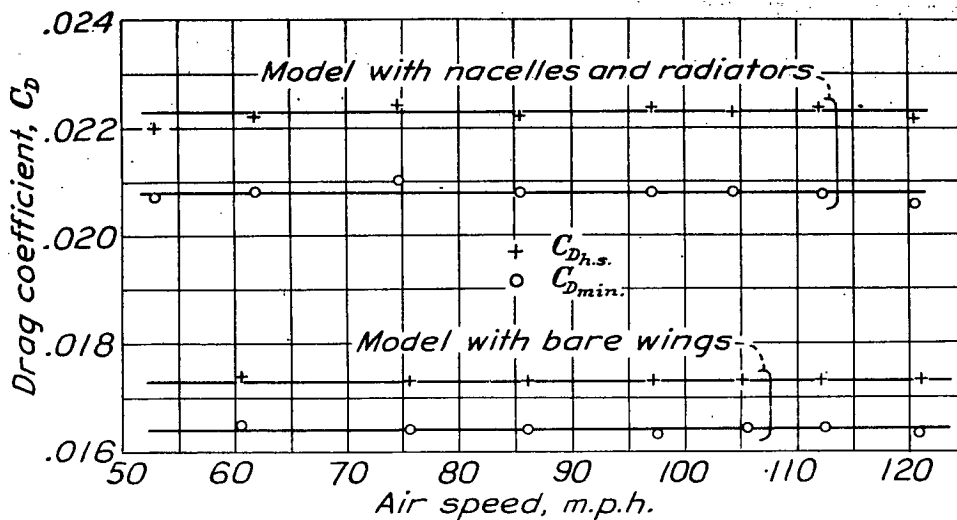


Figure 19

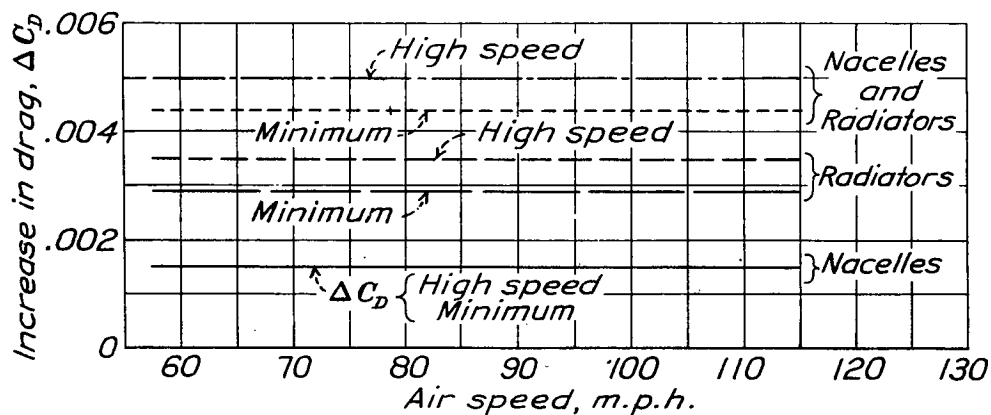


Figure 20

N.A.C.A.

Figs. 21, 22, 23

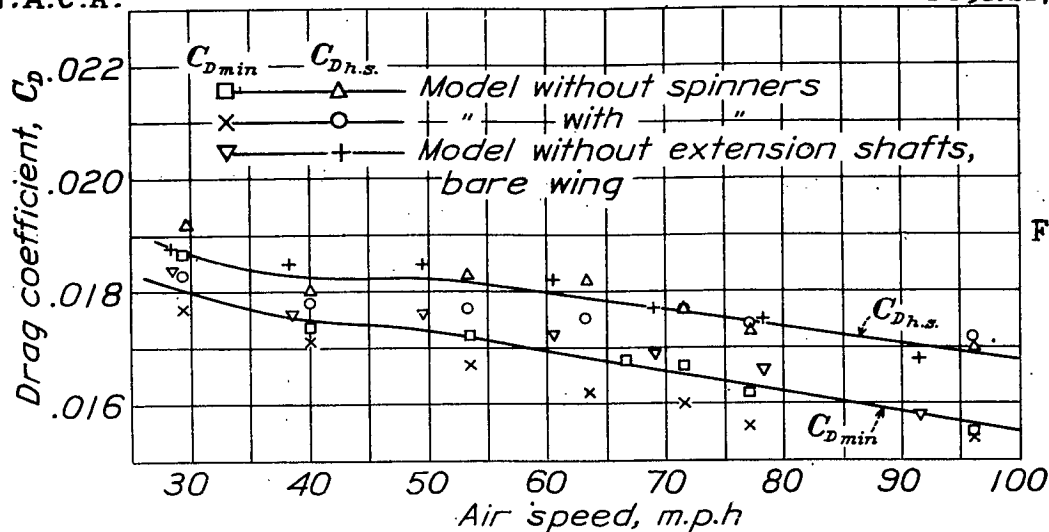


Fig. 21

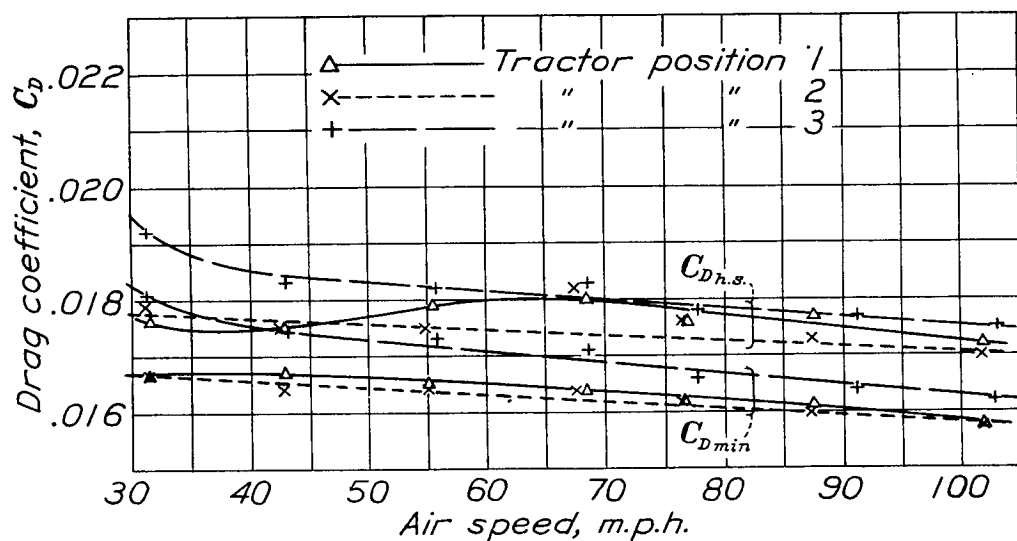


Fig. 22

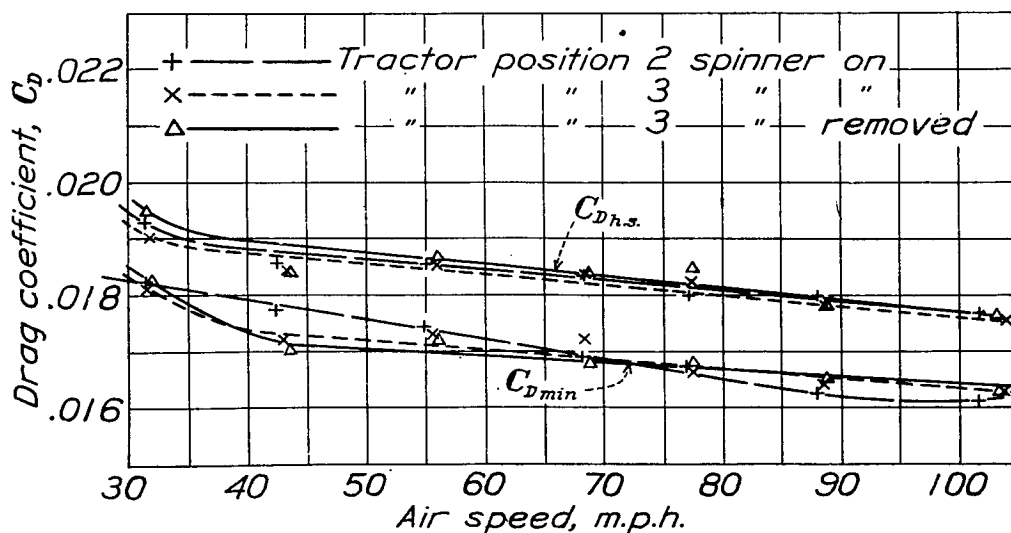
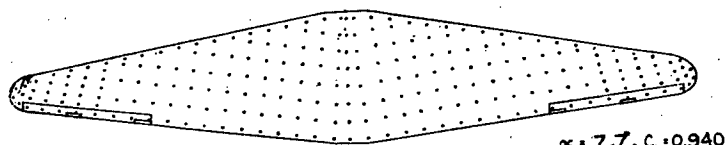
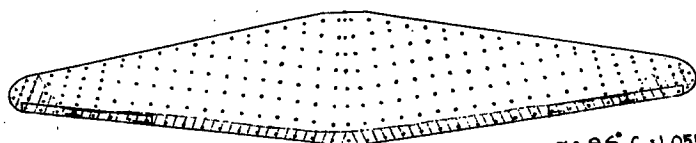


Fig. 23

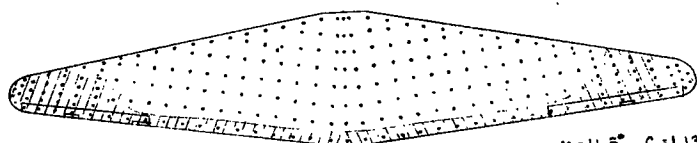
N.A.C.A.



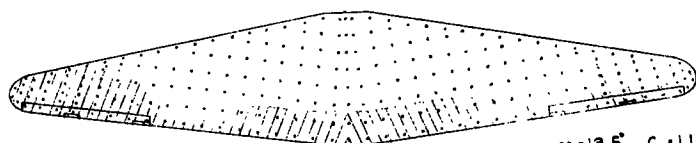
$\alpha_f = 7.7^\circ, C_L = 0.940$



$\alpha_f = 9.6^\circ, C_L = 1.055$



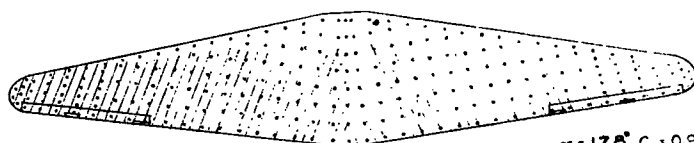
$\alpha_f = 11.5^\circ, C_L = 1.138$



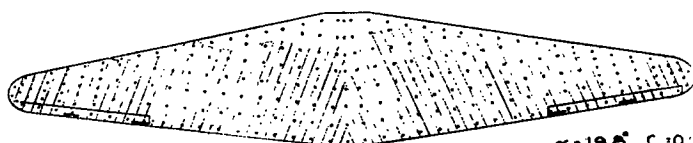
$\alpha_f = 13.5^\circ, C_L = 1.160$



$\alpha_f = 15.6^\circ, C_L = 1.162$



$\alpha_f = 17.8^\circ, C_L = 0.93$



$\alpha_f = 19.8^\circ, C_L = 0.7$

N.A.C.A.

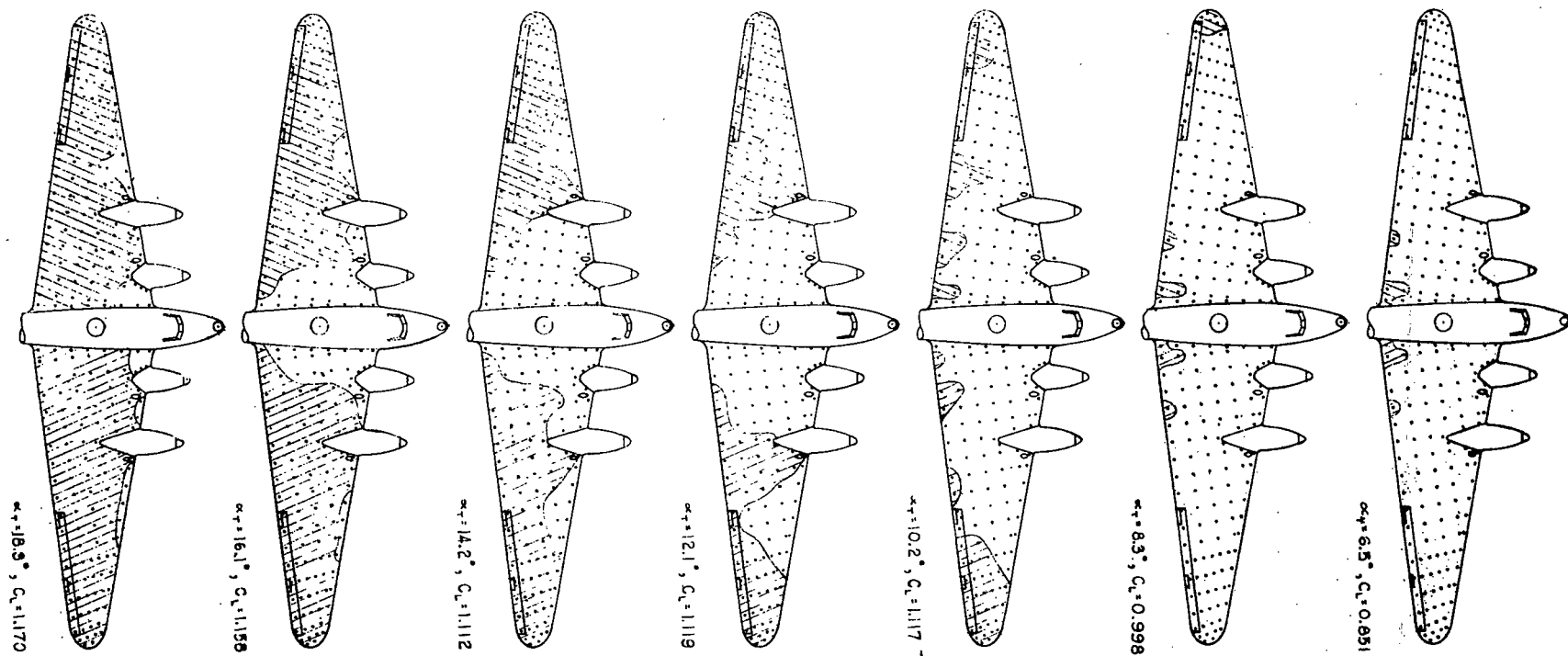


Figure 25. - Tuft surveys for the conventional wing-nacelle model. $\delta_e, 0^\circ$; $\delta_f, 0^\circ$; approx. test air speed, 50 m.p.h.

Fig. 25

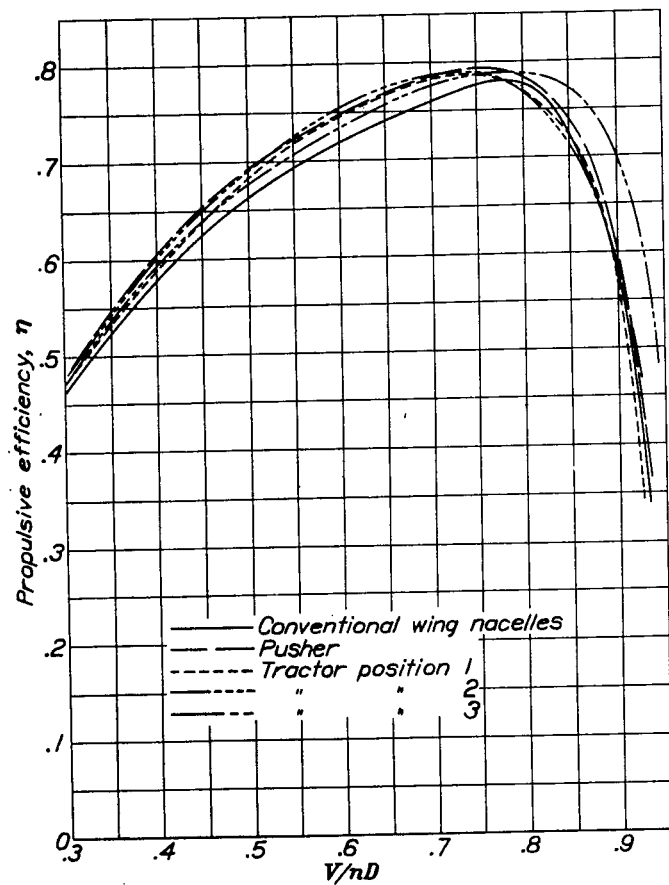


Figure 26

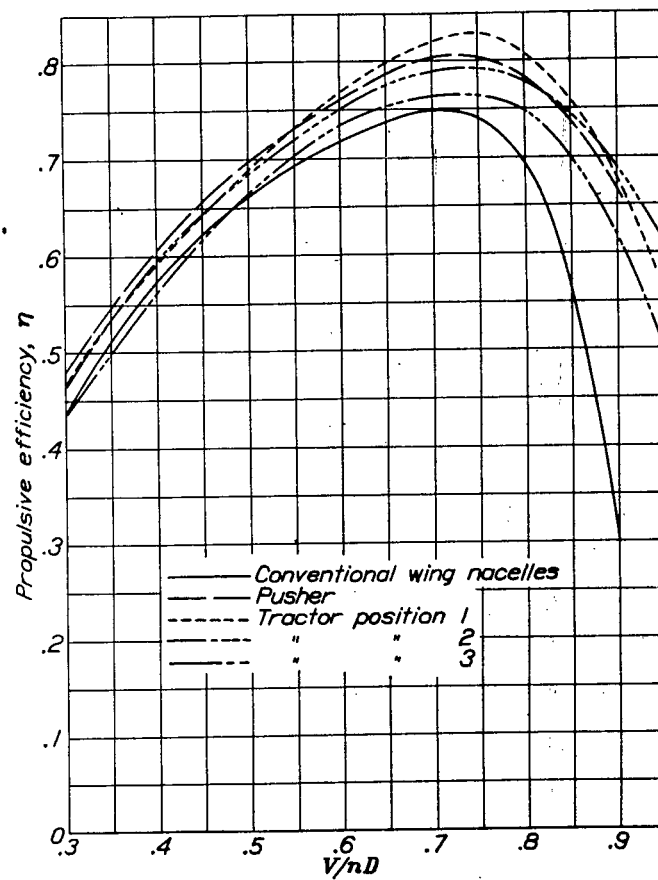


Figure 27

N.A.C.A.

Figs. 26, 27

N.A.C.A.

Figs.28,33

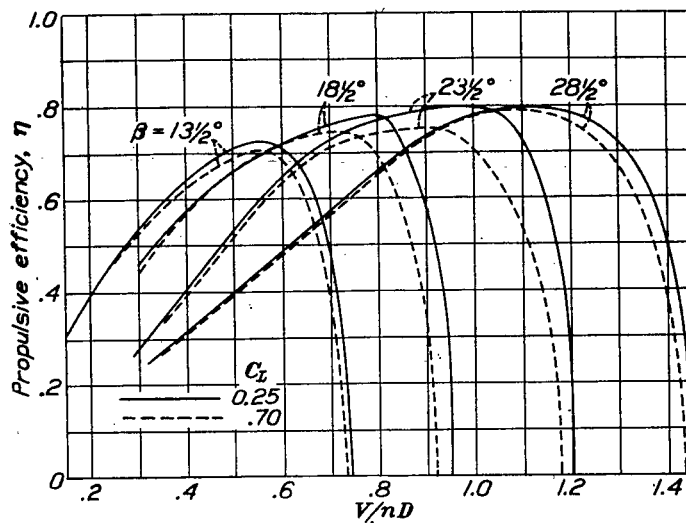


Figure 28

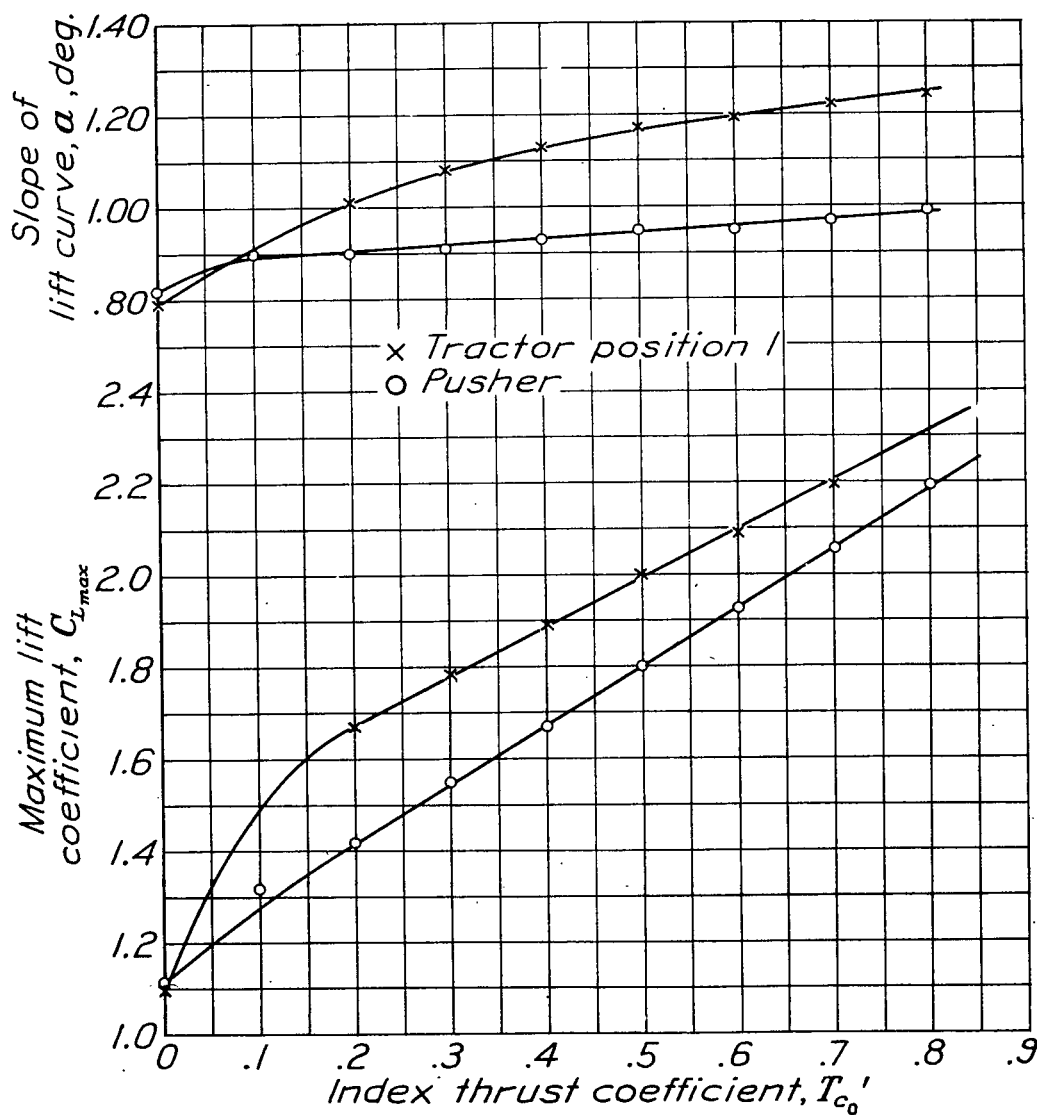


Fig.33

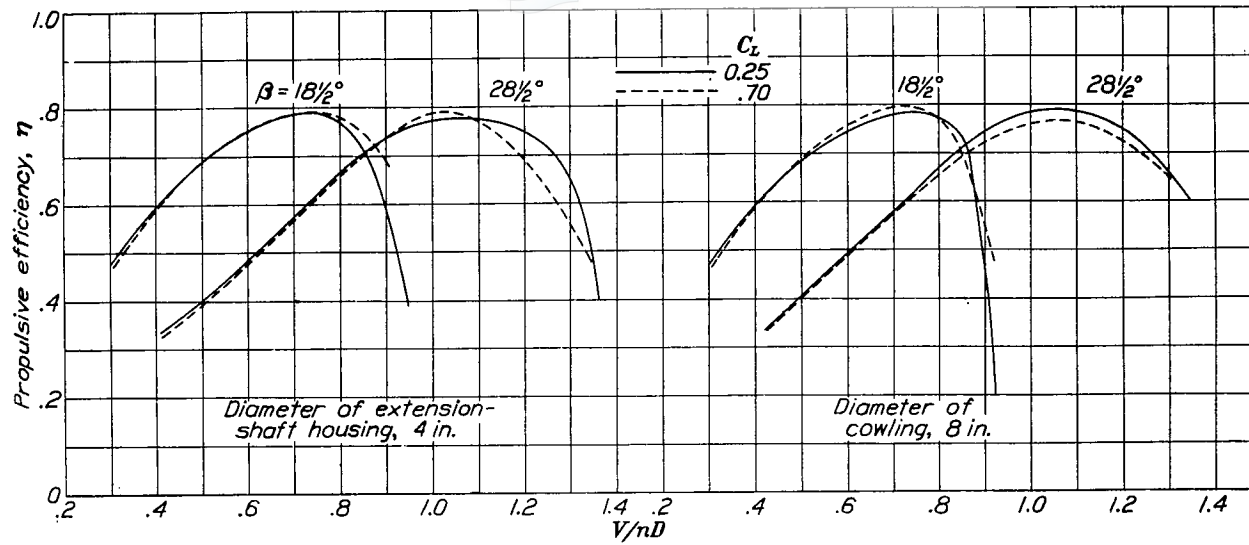


Figure 29

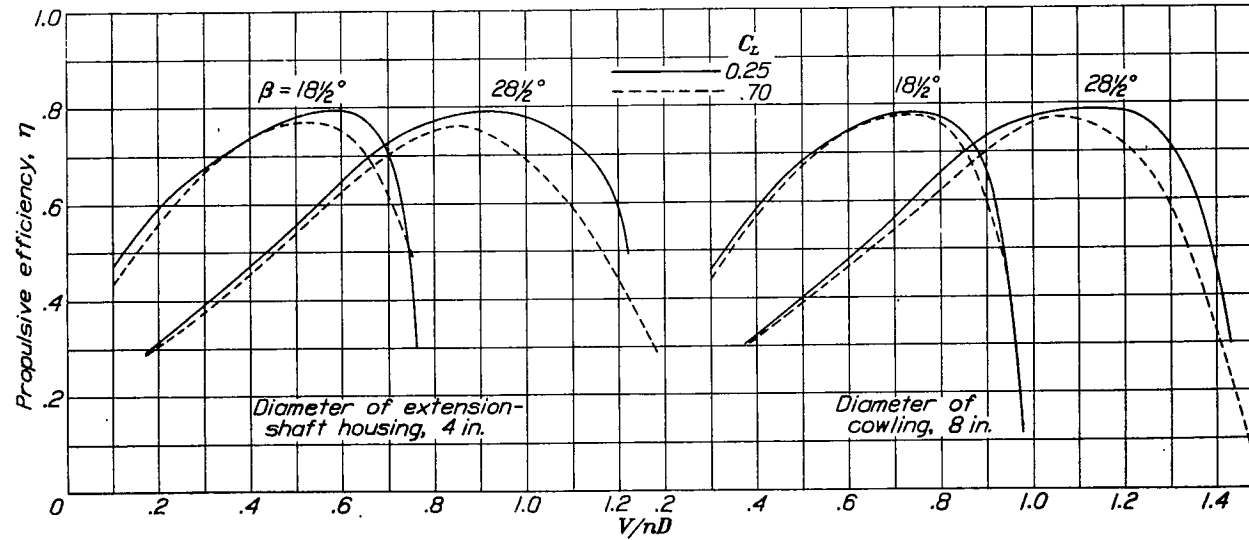


Figure 30

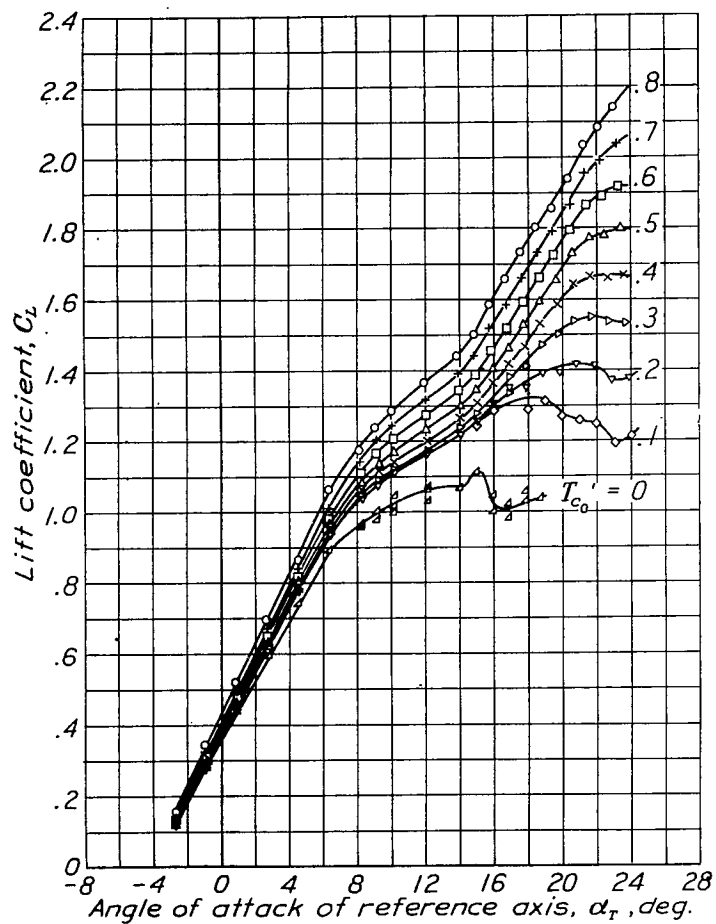


Figure 31

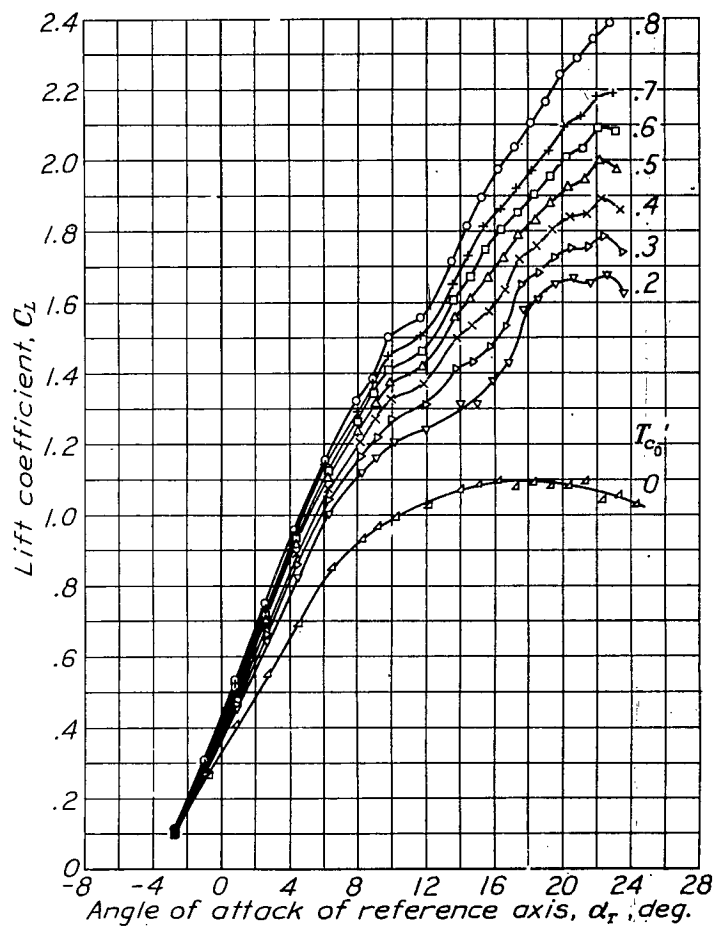


Figure 32

N.A.C.A.

Figs. 34.35

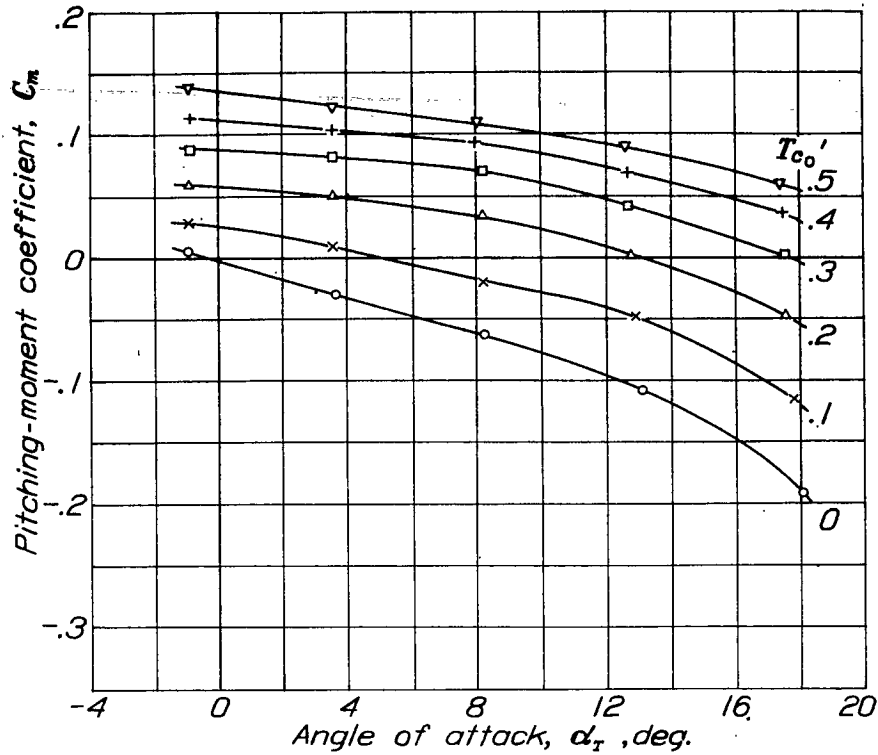


Figure 34.

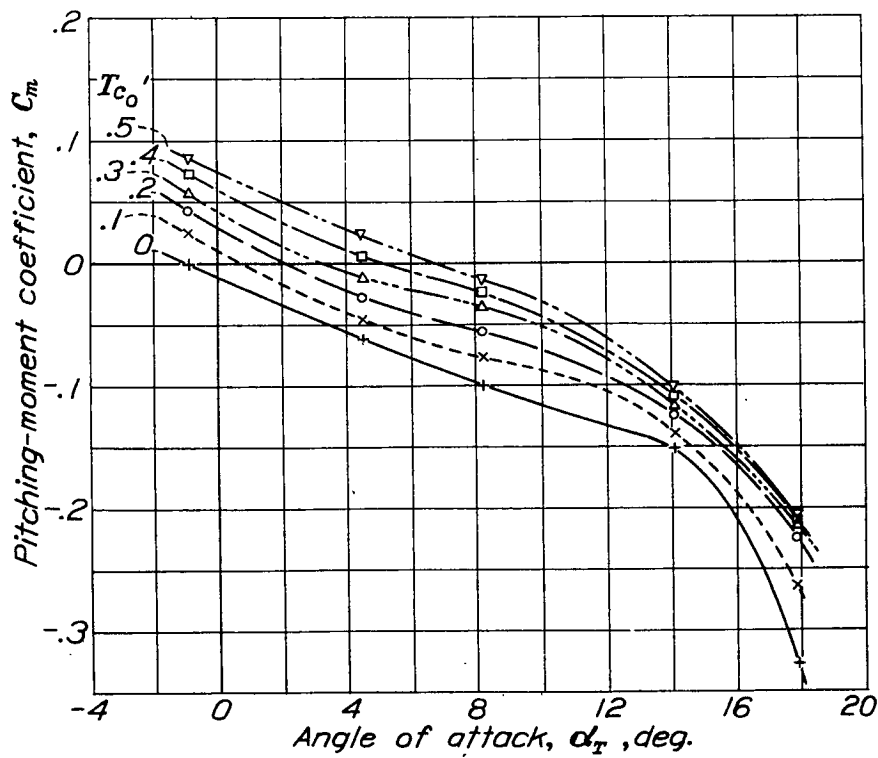


Figure 35.

Figure 37.- Comparison of high-speed computations for the wing-nacelle and the pusher models showing the effect of enclosing engines and radiators within the wings. Wing loading, 25.7 pounds per square foot; power loading, 17.7 pounds per horsepower, β , $18\frac{1}{2}^\circ$; standard sea-level density; δ_o , 0° ; δ_f , 0° .